G-33-A75
#3

Dr. Philippe Cran
Solar System Exploration Division
Office of Space Science
NASA Headquarters
Washington, DC 20546-0001

April 27, 2006

Dear Dr. Philippe Crane,

You will find enclosed my final report for the final year of grant NAG5-13234 entitled "Contributions of non-thermal surface processes to the formation of planetary atmospheres." We officially began this program on May 1, 2003. Please let me know if any additional information is required.

Sincerely,

Thomas M. Orlando
Professor and Chair
School of Chemistry and Biochemistry
Georgia Institute of Technology
(404) 894-4012
FAX (404) 894-7452
Thomas.Orlando@chemistry.gatech.edu

CONTRIBUTIONS OF NONTHERMAL SURFACE INTERACTIONS TO THE FORMATION OF PLANETRAY ATMOSPHERES IN THE OUTER SOLAR SYSTEM

FINAL REPORT

NASA Grant NAG5-13234
Georgia Tech Project G-33-A75
Deliverable No. 3
Performance Period: May 1, 2003 – April 30, 2006

Submitted to:
National Aeronautics and Space Administration
NASA Planetary Atmospheres Program
NASA Headquarters
Washington, DC 20546-0001
Attn: Dr. Philippe Crane

Submitted by: School of Chemistry and Biochemistry
Georgia Institute of Technology
Atlanta, GA 30332-0400

Principal Investigator: Dr. Thomas M. Orlando
Professor and Chair, School of Chemistry and Biochemistry
Adj. Professor, School of Physics
Ph: 404-894-4012
e-mail: Thomas.orlando@chemistry.gatech.edu

TABLE OF CONTENTS

SUMMARY PROGRESS

The non-thermal generation of tenuous atmospheres within the Jovian and Saturnian systems depends critically on electron and vacuum ultraviolet photon interactions with the low-temperature icy surfaces. The composition of these icy surfaces exhibits a broad range of impurities ranging from hydrated ionic salts to organic compounds. The presence and persistence of specific chemical entities such as minerals and salts also have important implications regarding the existence of putative sub-surface oceans on Ganymede and Europa. Thus, understanding the sources and compositions of their tenuous atmospheres requires knowledge not only of pure ice, but of the interaction of ice with soluble and insoluble impurities.

During the first year of grant NAG5-13234, we acquired infrared reflectance spectra of flash frozen acid and brine/ices that yielded essential clues to the surface composition of Europa. We then discovered an important relationship between the radiolytic production of atmospheric species at ice defects and the trapping of these products within clathrate hydrate structures that then become new sources of impurities in ice. This relationship is intimately related to the radiation induced production of molecular hydrogen and oxygen, two very important species which have been observed in the atmosphere of Europa. During the second and third year, we demonstrated important relationships between ice porosity, gas trapping and defects that mediate non-thermal production of atmospheric gases about icy bodies. In particular, we have found (i) a correlation between quiescent retention of radiolytic generated atmospheric gases and the migration of electronic excitations through ice, (ii) made continued progress in modeling the kinetics of ice radiolysis and radiation induced defect-mediated processing of ice, and (iii) applied this model to understanding near-threshold vacuum ultraviolet photon induced production of H_2 and O_2.

In summary, we have (i) acquired infrared reflectance spectra of flash frozen acid and brine/ices that yield essential clues to the surface composition of Europa, (ii) developed important refinements to the model of non-thermal production of O_2 on Europa, (iii) examined the roles of pores and ice structure on the non-thermal production and release of H, H_2 and O_2 from low-temperature ice and (iv) made significant improvements to our experimental apparatus used for electron- and photon-induced processes on icy surfaces.

1. Infrared Reflectance Spectra of Europa Surface Surrogates.

The icy moon Europa has been the subject of much scrutiny and recently there have appeared dissenting opinions on the interpretation of the near infrared reflectance spectra of the non-ice regions on Europa. Features observed in the 1-3 μm region can be attributed to overtone and combination bands of water that are perturbed by the presence of species other than neighboring water molecules. The non-ice or perturbed absorption features in near infrared mapping spectrometer (NIMS) data were initially attributed to the presence of heavily hydrated minerals such as magnesium and sodium sulfates from an endogenous source. Very good spectral matching was later obtained for sulfuric acid hydrates that may be produced by a radiolytic sulfur cycle that depends upon complex

radiation chemistry. Later work demonstrated that perhaps better agreement with NIMS spectra can be obtained when flash-freezing aqueous brines onto a very cold substrate in high vacuum [McCord et al., 2002]. It was suggested that the best fit should contain sulfuric acid and it was assumed that flash-freezing under high vacuum mimics the conditions typical of upwelling in fractures in the icy crust of Europa. This rapid quenching/glass forming process also preserves the water structures associated with solvated ions. It is precisely these complicated solvation structures formed during the flash-freezing of aqueous solutions that give rise to the optical signatures observed in the NIMS spectra. Figure 1 shows the spectra obtained for a series of selected flas-frozen sulfate bearing salts.

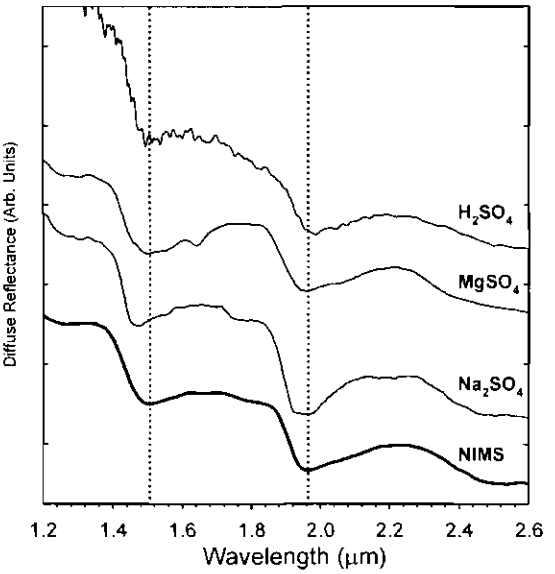

Figure 1: Infrared reflectance spectra of flash-frozen sulfate bearing salts compared to the NIMS result for a dehydrated region of Europa.

The best match to the NIMS spectra is a mixture of Na_2SO_4, H_2SO_4 and some $MgSO_4$. The data indicates that as much as 40 weight % of Na_2SO4 can be present and brackets the geochemical models developed to describe the evolution of Europa. Thus, we contend that the non-ice regions are likely comprised of mixtures of solvated salts, some of which act as proton sources.

The general stability of some sulfate salts to damage initiated by ionization and electronic transitions was previously investigated by our group and it was shown that metal sulfates were found to be especially stable [McCord et al., 2001]. However, radiation processing of a frozen brine containing singly-charged Na^+ might provide a source for the atomic Na that has been observed coming off the surface of Europa [Brown and Hill, 1996, Johnson, 2000; Cooper et al., 2001]. We are still investigating this possibility by examining the absolute yields and velocity distributions of the neutral Na desorption products released from electron-beam irradiated flash-frozen brines contain Na_2SO_4 and H_2SO_4.

2. Molecular Oxygen Precursor Model.

Understanding how O_2 might be formed from low-temperature ice is crucial for theoretical and experimental simulations of the surfaces and atmospheres of icy bodies in the outer Solar System [Hall et al., 1995; Sieger et al., 1998, and Orlando and Sieger, 2003]. Molecular oxygen is formed by direct excitation and dissociation of a stable precursor molecule, rather than (as has been previously thought) by diffusion and chemical recombination of precursor fragments. This precursor may not be unique, however, and production of O_2 may proceed via branched routes.

The production of O_2 is also dependent upon the temperature and phase of the ice. This is shown below in Figure 2.

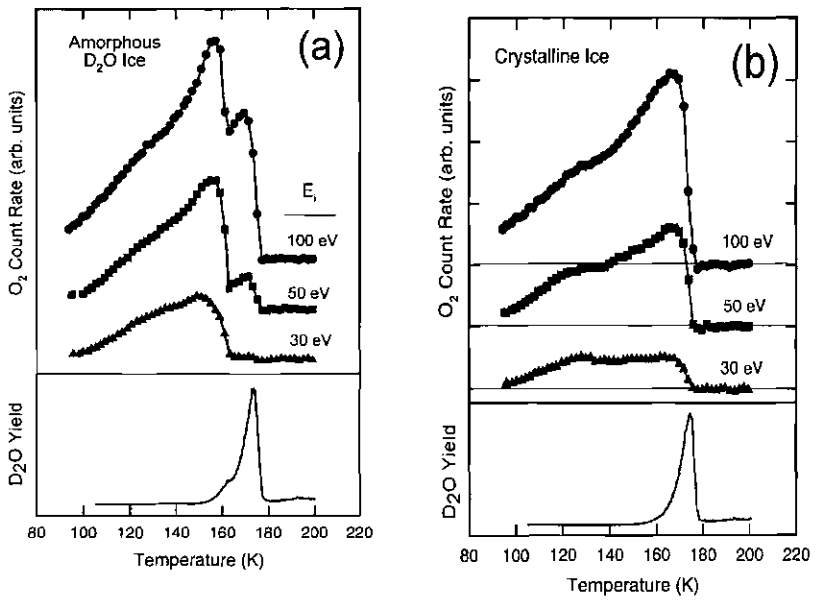

Figure 2: Temperature and phase dependence of O_2 production during the low-energy electron irradiation of ice.

We have also correlated the production and release of atomic and molecular hydrogen with the production of molecular oxygen. Formation of hot hydrogen molecules is associated with production of atomic oxygen and the production of hydrogen equilibrated to the ice surface temperature is correlated with the formation of thermalized molecular oxygen. Precursor formation is initiated by an electronic excitation of ice itself and this initial precursor is likely a trapped O-atom in an oxywater configuration. This species is metastable and may act as a precursor to molecular oxygen

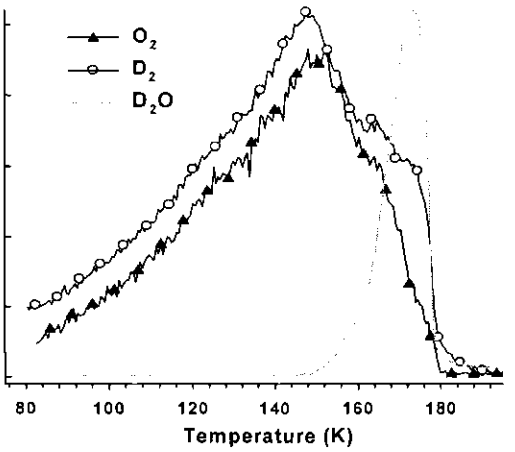

Figure 3: Temperature and phase dependence of O_2 production during the low-energy electron irradiation of ice.

or it may isomerize to form a secondary more thermodynamically stable product. One suggestion for this secondary isomerized product is hydrogen peroxide, which has been observed in optical reflectance measurements on Europa [Carlson et al., 1999]. We have contributed to the development of a solid-state chemical model for the production of O_2 by electronic excitation of ice. This model includes competition with precursor destruction and the effect of sample phase. This allows us to put the UV photon, low energy electron and fast ion experiments on a common footing for the first time. At low temperatures, the formation of the trapped oxygen atom precursor is favored by the preferential loss of molecular hydrogen and is quenched by reactions with mobile H. The presence of impurity scavengers can limit the trapping of O, leading to the formation of oxygen-rich molecules in ice. Rate equations that include these reactions were developed and then integrated to obtain an analytic approximation for describing the results of experiments on the production and loss of molecular oxygen from ice samples. In the proposed model, the loss rate varies, roughly, inversely with solid-state defect density at low temperatures, leading to a yield that increases with increasing temperature as observed. Cross sections obtained from fits of the model to laboratory data are evaluated in light of the proposed solid-state chemistry.

3. The Importance of Porosity and Ice Phase on Non-thermal Desorption and Planetary Atmosphere Formation.

The generation of tenuous atmospheres around icy moons by high energy radiation is well established. High quality measurements of Europa and Ganymede by the Hubble Space Telescope and the Galileo mission combined with careful laboratory studies have proven that non-thermal processing of the cold ice surface is responsible for

much of the tenuous atmosphere surrounding these moons. The latest data from the Cassini mission reveals that this processing is not specific to Jupiter's moons, but rather is quite general, occurring even in the icy ring system of Saturn. Preliminary infrared spectra from this probe has revealed that the moon Enceladus is completely covered by a relatively pure and young ice surface, and it anticipated that many more of Saturn's moons will be icy. Laboratory measurements until now have concentrated on the immediate ejection of gaseous products into the vacuum from direct irradiation of photons, electrons and fast ions. An important factor in gas or vapor phase generation of atmospheric components is the range of thermal cycling the planetary body undergoes. Radiolytic yields have temperature behavior that map either directly or inversely onto the hydrogen bonding strength of ice. We have found, however, that an additional source term can be a result of gas build up during low temperature phase of the cycle, followed by explosive release during the warm phase. So, while radiation exposure often cycles with the thermal cycling of a planetary body, the apparent yields can also depend on the history of exposure through at least one sidereal day.

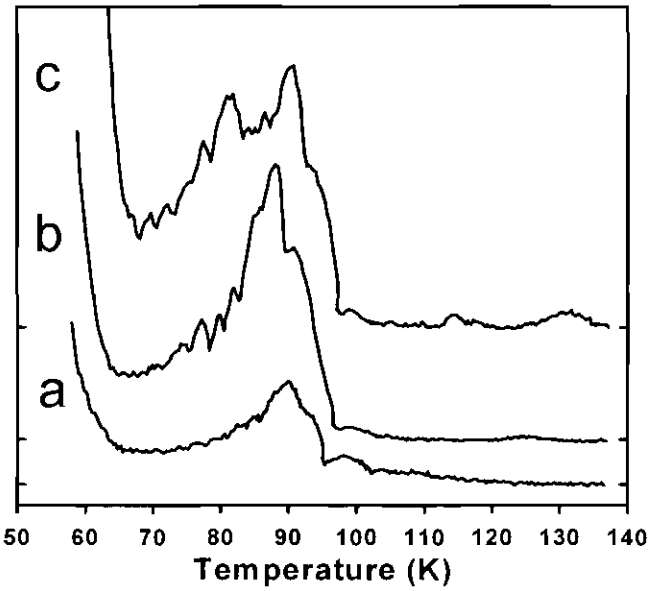

Figure 4: Post-irradiation release of molecular hydrogen upon warming. The plots are (a) crystalline ice, (b) amorphous and (c) highly porous amorphous ice. Porous ice exhibits a characteristic burst of trapped hydrogen release (80 K) when the internal pressure of the "bubble" bursts.

The yields of trapped molecular products were studied by (a) preparing ice in a controlled phase, (b) irradiating the ice with 100 eV electrons at controlled temperature, and then (c) perform Temperature Programmed Desorption measurements with a mass spectrometer. We have observed molecular hydrogen escape at low temperatures using this technique and found that it is released at relatively low temperature, shown in Figure 4, primarily because the molecules are small enough to fit through small interstices in the lattice and between grains in polycrystalline phases. Trapping of these products is an indication that the defect sites involved in the radiation chemistry are closely related to

structural defects that form microscopic pockets, such as clathrates or pores. Highly porous ice shows a striking and distinct feature which is the result of gaseous products trapped within the pore cavity, that explodes upon warming and expanding. Molecular oxygen shows a different result, where it is retained in the ice to much higher temperatures (not shown). This is a result of both the larger size the molecule, limiting the types of trapping sites possible for it, but also due to differences in the types and locations of the defects responsible for its production. This has far reaching implications, not only for planetary bodies but also for other warming ices such as interstellar icy grains near newborn stars and approaching comets.

The initial radiation must create excitations at the defect sites responsible, however the penetration depth of the radiation used here is much smaller than the thickness of the films. This tells us that another mechanism must be at work for the transfer of electronic energy though the lattice. This measurement supports our notion that long range energy transport can play a significant role in delivering energy to the sites where radiolytic activity can ensue. We are continuing the pursuit of mapping out the detailed structural origin of these effects using mixed ices. Defect sites can be inserted by doping flash frozen salt brines or organic molecules. Altering the nascent distribution of defects will modulate the resulting product yields, either amplifying or quenching them.

4. Production of Hydrogen and Oxygen Using Sub-Bandgap UV Photons.

As we have shown, defects in the ice matrix are the quintessential factor in the radiochemistry of icy surfaces. Pure ice possesses an intrinsic defect density, as evidenced by its nonzero entropy even at zero K, and can be made very high by control of the deposition process. Pure ice has a bandgap of about 7 eV, but exhibits what's known as an Urbach tail which tapers off to much lower energy. This tail is the result of an inhomogeneous distribution of defects that introduce electronic states within the bandgap, thus effectively diminishing it. Photon excitation below the bandgap, therefore, should selectively excite the defects of ice while not exciting bulk ice for lack of sufficient energy. We have utilized the technique of post-irradiation TPD, described above, to improve our sensitivity of detection near threshold by virtue of the storage effect to detect these low energy products.

Figure 5 shows the molecular oxygen TPD of ice irradiated with 6.2 eV photons. As stated above, molecular oxygen is trapped in ice until near the temperature of sublimation, owing to its increased sticking coefficient over hydrogen. These preliminary results indicate that the total cross section for O_2 production at low energy is dominated by the cross section of these sub-bandgap defect states. More precise measurements of this phenomena should allow us to extract quantitative values of cross sections and defect density of ice. Once this is established, we will have a benchmark for quantifying the degree of defectiveness of the phases of ice and of impurity states therein.

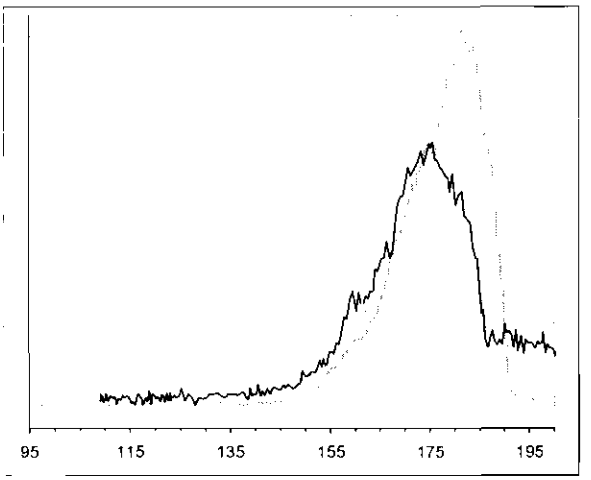

Figure 5. Post-irradiation TPD of molecular oxygen created by VUV photons at the threshold for production (6.2 eV). The dark line shows release of trapped O_2, while gray line is the TPD of ice.

5. Improvements to the apparatus.

We have two state-of-the art ultrahigh vacuum systems for the measurement of absolute cross sections for electron and photon-induced desorption of atomic and molecular products from low temperature ice surfaces. We have improved one of these systems to

i.) Allow us to flash-freeze salt solutions while maintaining extremely good vacuum conditions.

ii.) Allow simultaneous measurement of infrared reflection/absorption spectra and non-thermal desorption

iii.) Allow deposition of organic aerosols to simulate photo-induced processes that may occur in Titan's atmosphere.

CONTRBUTIONS TO STUDENT EDUCATION

This grant provided full support for post-doctoral fellow Dr. Greg Grieves and partial support of the thesis work of Dr. Janine Herring-Captain and Mr. bide olanrewaju. Dr. Greg Grieves is currently a Research Scientist at Georgia Institute of Technology, Dr. Herring-Captain is currently a full time Research Scientist at the Kennedy Space Center, and Mr. is continuing his thesis work with NASA support.

PUBLICATIONS AND PRESENTATIONS ACKNOWLEDGING SUPPORT FROM NASA GRANT NAG5-13234.

Publications:

T. M. Orlando, T. B. McCord, G. A. Grieves, "The Chemical Nature of Europa Surface Material and the Relation to a Sub-Surface Ocean." *Icarus* 177 (2005) 528-533.

R. E Johnson, P. D. Cooper, T. Quickenden, G. A. Grieves and T. M. Orlando, "Production of Oxygen by Electronically-Induced Dissociations in Ice." *J. Chem. Phys.* 123 (2005) 1847115.

G. A. Grieves, T. M. Orlando, "The Importance of Pores in the Electron Stimulated Production of H_2 and O_2 in Low Temperature Ice." *Surface Science* 593 (2005) 180-186.

T. M. Orlando, T. B. McCord, G. A. Grieves, A. B. Alexandrov and J. H. Herring, "The Chemical Nature of the Galilean Satellite Non-Ice Spectral Signatures" *In preparation, Icarus..*

G. Grieves, G. A. Kimmel, and T. M. Orlando, "The Kinetics and Temperature Dependence of Atomic Oxygen Formation via Low-Energy Electron Bombardment of Ice.", *In preparation, J. Chem. Phys.*

Presentations:

Non-thermal Processes on Low Temperature Ice Surfaces and the Relevance to Planetary Atmospheres, G. Grieves, T.M. Orlando, J. Herring and A. Aleksandrov, Invited Talk, RIKEN (The Institute of Physical and Chemical Research) Wako, Saitama Japan December 7, 2003.

Surface Processes On The Icy Moons Of Jupiter From Interplanetary Radiation Bombardment, G. Grieves, A. Alexandrov, J. Herring and T. M. Orlando, 55th Southeast Regional Meeting of the American Chemical Society, Atlanta, GA, November 26, 2003.

Hydrated Materials on Europa's Surface: Review of Current Knowledge and Current Results, T. McCord, T. M. Orlando, G. B. Hansen and C. A. Hibbitts, Workshop on Europa's Icy Shell: Past, Present and Future, Houston, Texas. February 6-8, 2004.

"Electronic desorption from 'surfaces' within pores of low temperature ice," G. A. Grieves, T. M. Orlando, Contributed Talk, DIET-10 Conference, Fuji Kyoiku Kenshu-jo, Japan, November 2004.

Composition of Europa's Icy Shell from the Galileo Near Infrared Mapping Spectrometer, G. Grieves, T.M. Orlando, T.B. McCord, South Eastern Laboratory Astrophysics Consortium (SELAC), University of Kentucky, Louisville, April 29, 2005.

Surface Processing on the Icy Moons Of Jupiter from Interplanetary Radiation Bombardment G. Grieves, T. M. Orlando, T. B. McCord, Invited Talk, Georgia State University, Department of Geology, Atlanta, GA, November 9, 2005.

The Oxygen Atmosphere of Jupiter's Icy Moons, G. Grieves, T.M. Orlando, R.E. Johnson, Invited Talk, Spring Hill College Chapter of the American Chemical Society, Spring Hill College Dept. of Chemistry, Mobile AL, March 31 2005.

References:

Brown, M.E., and R.E. Hill, Discovery of an extended sodium atmosphere around Europa, *Nature (London)*, *380*, 229-31, 1996.

Carlson, R.W., M.S. Anderson, R.E. Johnson, W.D. Smythe, A.R. Hendrix, C.A. Barth, L.A. Soderblom, G.B. Hansen, T.B. McCord, J.B. Dalton, R.N. Clark, J.H. Shirley, A.C. Ocampo, and D.L. Matson, Hydrogen peroxide on the surface of Europa, *Science (Washington, D. C.)*, *283* , 2062-2064, 1999.

Cooper, J.F., R.E. Johnson, B.H. Mauk, H.B. Garrett, and N. Gehrels, Energetic ion and electron irradiation of the icy Galilean satellites, *Icarus*, *149* (1), 133-159, 2001.

Hall, D.T., D.F. Strobel, P.D. Feldman, M.A. McGrath, and H.A. Weaver, Detection of an oxygen atmosphere on Jupiter's moon Europa, *Nature (London)*, *373*, 677-9, 1995.

Johnson, R.E., Sodium at Europa, *Icarus*, *143* (2), 429-433, 2000.

McCord, T.B., T.M. Orlando, G. Teeter, G.B. Hansen, M.T. Sieger, N.G. Petrik, and L. Van Keulen, Thermal and radiation stability of the hydrated salt minerals epsomite, mirabilite, and natron under Europa environmental conditions, *J. Geophys. Res., [Planets]*, *106* (E2), 3311-3319, 2001.

McCord, T.B., G. Teeter, G.B. Hansen, M.T. Sieger, and T.M. Orlando, Brines exposed to Europa surface conditions, *J. Geophys. Res., [Planets]*, *107* (E1), 4/1-4/6, 2002.

Sieger, M.T., W.C. Simpson, and T.M. Orlando, Production of O2 on icy satellites by electronic excitation of low-temperature water ice, *Nature (London)*, *394* , 554-556, 1998.

T. M. Orlando and M. T. Sieger, "The Role of Electron-Stimulated Production of O2 from Water Ice in the Radiation Processing of Outer Solar System Surfaces, *Surf. Sci. 528,1,* 2003.

Available online at www.sciencedirect.com
SCIENCE DIRECT®
Surface Science 593 (2005) 180–186
SURFACE SCIENCE
www.elsevier.com/locate/susc

The importance of pores in the electron stimulated production of D_2 and O_2 in low temperature ice

Gregory A. Grieves [a], Thomas M. Orlando [a,b,*]

[a] School of Chemistry and Biochemistry, Georgia Institute of Technology, Atlanta, GA 30332-0400, USA
[b] School of Physics, Georgia Institute of Technology, Atlanta, GA 30332-0400, USA

Available online 18 July 2005

Abstract

The effects of porosity and morphology of amorphous and crystalline D_2O ices on the electron stimulated generation and trapping of D_2 and O_2 have been studied by post-irradiation thermal desorption. The trapped product yields increase from crystalline ice to amorphous ice to highly porous amorphous ice, similar to observed ESD yields. This is attributed to the increased number of defects, traps and pores in amorphous ice. Molecular deuterium is released in the temperature range from 55 to 105 K for each of the samples, with two notable bursts at 115 and 132 K for porous amorphous ice. Low temperature release is associated with diffusion of D_2 through micropores in the ice matrix. Highly porous amorphous ice shows a striking spike in the release of D_2 at 80 K which has not previously been observed and must be a result of trapping of D_2 within enclosed macropores. The trapped D_2 in macropores may result from transport of excitation energy to the pore interface or from transport of D_2 through micropores at lower temperatures during TPD, or both. Molecular oxygen is retained within ice until much higher temperatures (>140 K). The release at this temperature is attributed to sintering and diffusion along grain boundaries in crystalline ice. The majority of trapped O_2 evolves with the desorption of the ice matrix, suggesting that clathrate hydrates may be important trapping sites. Amorphous ice releases a surge of trapped O_2 at the 160 K amorphous to crystalline phase transition, which is consistent with codeposition experiments. Highly porous ice exhibits much higher total yields of oxygen and shows a second strong spike in trapped O_2 release at 175 K.

Keywords: Electron stimulated desorption; Electron induced reactions; Water; Ice; Hydrogen; Oxygen

1. Introduction

Transformations of the structure of amorphous ice are tremendously important for the understanding of physical chemical processes in low

* Corresponding author. Address: School of Chemistry and Biochemistry, Georgia Institute of Technology, Atlanta, GA 30332-0400, USA. Tel.: +1 404 894 8222; fax: +1 404 894 7452.
E-mail address: thomas.orlando@chemistry.gatech.edu (T.M. Orlando).

0039-6028/$ - see front matter © 2005 Elsevier B.V. All rights reserved.
doi:10.1016/j.susc.2005.06.059

temperature environments of interstellar space, icy planetary bodies and outer solar system remnants such as comets and trans-neptunian objects [1–5]. Ices in these environments are never pure and occur in complex mixtures with other abundant molecules. A special property of porous amorphous ice is its ability to trap condensates on and within the ice framework as clathrate hydrates and within micropores and cavities formed from long needle-like crystallites [6–10]. Thermal desorption experiments of gases codeposited with ice have proven to be extremely sensitive probes of ice structural reorganization, and show several distinct temperature ranges of trapped gas release [6,7]. This has important ramifications for the astrophysics of icy grains, for example, since trapped products within pores could significantly modify the predictions of outgassing of ices in warming protostellar regions beyond the simplified surface adsorption model.

Ices in astrophysical environments, however, are often subject to high energy radiation bombardment. Radiation induced desorption from low temperature water ice plays a crucial role in the astrochemistry of icy planetary surfaces [11–14], comets (e.g., [15]) and ice-covered interstellar grains (e.g., [16]). Excitations from low energy secondary electrons can migrate along the strongly coupled hydrogen bonding network until they encounter a surface or a defect where they can localize and induce dissociation [17–19]. The electronic structure of ice at the interface of large porous cavities in amorphous ice may resemble that of the free surface interface, and therefore it might be expected that ESD processes would occur there with similar mechanisms. Neutral products from low energy (5–250 eV) electron bombarded low temperature ice include H(D), $H_2(D_2)$, $O(^3P, ^1D)$, O_2, $H_2O(D_2O)$ and $H_2O_2(D_2O_2)$ and progress has been made in understanding their respective production mechanisms [17,20–23]. For instance, molecular hydrogen with non-thermal translational energy distributions has been shown to originate purely from exciton decay at the vacuum surface interface and more recently at the substrate interface [20,22]. The mechanisms seem to involve energy or charge transport followed by recombination and unimolecular dissociation. Molecular oxygen, however, requires a pair of water molecules to form and has been shown to require a minimum ice film thickness of 2 ML to be produced. The yields are also affected by the defect density of the ice [14,24–26]. It has been suggested that molecular oxygen is present in condensed form on the icy surfaces of Europa, Ganymede and Callisto, known to be produced by radiolysis from the high radiation flux near Jupiter [27]. However, no experiments have yet to address this issue of O_2 trapping using low energy electron bombardment and post-irradiation thermal desorption.

In this paper, we report our first results on a program focused on the role of pores in stimulated reactions within low temperature ice. To examine the interaction of large scale structural configurations of amorphous ice on the stimulated desorption of molecular products, we have measured the yields and release of D_2 and O_2 in post-low-energy electron beam irradiation thermal desorption studies of porous D_2O ice.

2. Experiment

The experiments were performed in a UHV chamber with base pressure 1×10^{-10} Torr, equipped with a pulsed electron gun and a quadrupole mass spectrometer (QMS). The electron beam has a typical current density of 10^{14} electrons/cm^2 s, and a beam spot size of $\sim$1.5 mm. The electron beam was pulsed at 1000 Hz, with a pulse width of 500 μs and was rastered twice over an area of about 0.5 cm^2 in 50 min. This was done to reduce the effects of short term surface charging and localized heating of the ice, while dosing enough area to average over spatial inhomogeneities and to accumulate enough material to detect. The incident electron energy used was 100 eV. The graphite substrate was mounted in thermal contact with a compressed helium cryostat and heated with a resistive button heater which allowed for temperature control from 55 to 500 K. The substrate temperature was monitored with a thermocouple mounted to the substrate and a computer-controlled feedback system drove the temperature ramp at a rate of 8 K/min. D_2O was used to discriminate against signal from background

H_2O. Porous amorphous solid water (PASW) samples were deposited at 50 K with a directional doser oriented approximately 70° from normal incidence. Non-porous amorphous solid water (ASW) samples were dosed at 120 K at normal incidence and crystalline ice (CI) samples were deposited between 150 and 155 K. Film thickness is estimated by comparison to published TPD data and is estimated to be between 50 and 100 ML, where 1 ML is defined as 1 s exposure to 1×10^{-6} Torr D_2O vapor. TPD spectra show a significant signal in the 4 AMU mass channel during desorption of D_2O due to gas phase electron impact dissociation inside the QMS ionizer. This prevents us from making conclusive statements about the evolution of D_2 from the ice surface in the temperature range above 140 K, but has no effect on the detection of the other products monitored in these experiments.

3. Results and discussion

3.1. Evolution of molecular deuterium from irradiated D_2O ice

Results of post-irradiation thermal desorption of D_2 are shown in Fig. 1 for (a) crystalline, (b) non-porous amorphous and (c) porous amorphous ice films grown on a graphite substrate. The ices were irradiated at 55 K; a temperature where defect mobility is low, but exciton and electron mobility, modulated by hydrogen bond strength, is expected to be high. There is a large initial burst of D_2 upon commencement of heating from 55 K up to 65 K which is due to physisorbed D_2 resulting from surface ESD during electron irradiation. Exposure of porous ice to D_2 below 60 K has been shown to adsorb large numbers of molecules, more than can be accounted for by effective surface area of ice [6]. This implies the adsorbed molecules penetrate beneath the surface through micropores [6].

For each of the ice films, there is a gradual rise in the amount of D_2 released in the temperature interval from 70 to 95 K, followed by a distinct drop where desorption is complete by about 100 K. Also evident is a small shoulder feature near 100 K present for all samples. For comparison, the TPD of physisorbed D_2 on graphite and codeposited with porous D_2O ice is shown in lower panel of Fig. 1. Desorption of D_2 from graphite shows a solitary peak near 73 K and is complete by 80 K under these TPD conditions. TPD from D_2 codeposited with D_2O shows an additional small feature at 90 K which is consistent with previous codeposition experiments and attributed to the restructuring of the amorphous ice due to the onset of defect mobility which could account for transport through the material. *In this temperature range, D_2 will not adhere to the outer ice surface, nor to any exposed graphite, therefore must originate within the ice.*

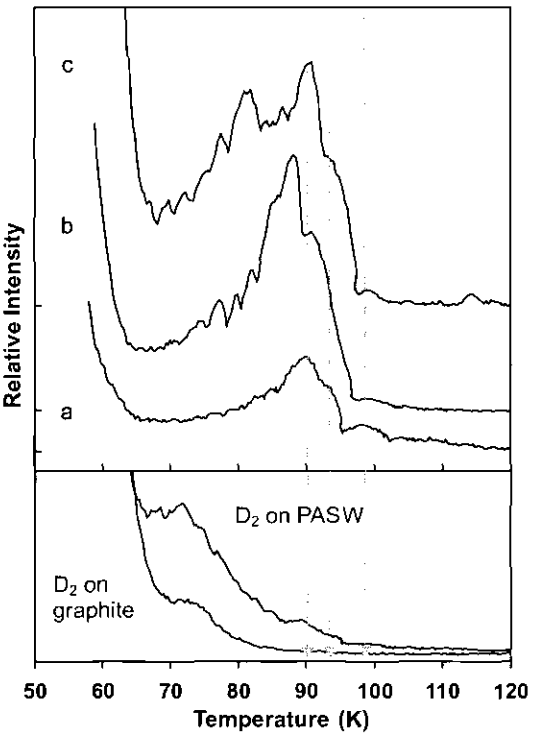

Fig. 1. Post-irradiation TPD spectra of (a) D_2O dosed at 150 K, (b) D_2O dosed at 120 K, and (c) D_2O dosed at 55 K. Irradiation of 100 eV electrons occurred at 55 K for all samples, then thermal desorption of D_2 was monitored. The inset below shows the TPD of D_2 adsorbed onto graphite (lower curve) and codeposited with porous ice (upper curve).

The release of trapped D_2 from irradiated crystalline ice is shown in Fig. 1, plot **a**. This plot shows three distinct features which are common

to all of the ices. The largest peak occurs at 93 K, accompanied by a shoulder at 95 K, and a small companion peak near 100 K. Close inspection reveals that each of these are also present in the TPD of D_2 codeposited with non-irradiated D_2O. These features may result either from differences in the trapping sites holding D_2 or from distinct physical transitions of the ice. Other experiments, such as calorimetry [1], have not revealed any structural transitions in this region. Thus, a likely possibility is that there are similar but subtly different types of trapping sites that have different strengths of retention for D_2. It is known, for instance, that clathrate hydrates can form in many polyhedral morphologies, including octahedral, dodecahedral and so on.

Comparison of the thermal desorption of D_2 from irradiated amorphous ice (ASW) grown at 120 K is shown as curve **b** in Fig. 1. The total amount of released D_2 is much higher than for crystalline ice and also exhibits a sharp peak around 88 K. The total ESD neutral product yields are generally much higher from amorphous ice than from crystalline. This is attributed to increased defect density and an increase in excitation localization due to disruption of long range order in the matrix [28]. This elevated defect density may also provide an increased density of trapping sites for D_2 within the matrix. The TPD of ASW is ostensibly the same as that for CI but scaled up for these two reasons.

The post-irradiation TPD of porous amorphous ice (PASW) deposited at steep incident angle at 55 K is shown in Fig. 1c. The general appearance is similar to that of ASW except for another distinct peak in yield at 85 K. Again, the total D_2 yields for this phase are significantly higher than either ASW or CI. *The presence of this additional peak can therefore be attributed to the presence of large porous volumes that trap D_2.* The presence of large pockets within the ice, we will call macropores, provides a surface area where D_2 could desorb from the interior walls and remain trapped. The macropores responsible for this observed peak must be fully enclosed and have no open path to the vacuum interface. At this temperature, however, D_2 cannot be physisorbed onto the ice. With increasing temperature, the gas pressure within these pockets may exceed their mechanical strength and burst the pore. As discussed above, D_2 can begin to migrate through micropores in the ice lattice near 60–65 K, some of which escape at the vacuum interface. These macropores act as an obstruction to both the transport of energy to the substrate interface, and to the diffusion of D_2 produced at the substrate interface out to the vacuum. Since the source of all D_2 observed is from pre-irradiation at low temperature, it is not possible to distinguish between D_2 which has migrated to the macropore through the micropores, or D_2 which has formed from localized excitation at the interior surface of the pore by energy transport. Both mechanisms are likely to occur.

3.2. Post-irradiation release of molecular oxygen

Molecular oxygen has been observed in or from the icy surfaces of Europa, Ganymede and Callisto. O_2 is known to be produced by radiolysis from the high radiation flux near Jupiter [27] and may exist trapped in condensed form. Monitoring the mass 32 (O_2) channel during post-irradiation TPD results in the spectra shown in Fig. 2. The overall yields of O_2 for each type of ice follow the pattern of CI < ASW < PASW. The yield for crystalline ice is shown as trace (a) in this figure, and shows the onset of trapped O_2 release near 140 K, which occurs significantly before the TPD of the ice, shown in gray underneath. Since O_2 production is correlated with defect density, and likely occurs in the near surface region, it should also be preferentially produced in internal defects such as grain boundaries. The release of O_2 during desorption of the ice matrix is a result of O_2 trapped within the lattice. This could possibly be as a clathrate hydrate, and correlates well with observations in codepostion experiments [6].

In contrast to CI, the results for ASW (Fig. 2b) show the appearance of a spike in yield at 160 K, which then continues to evolve in correlation to the TPD of the ice. This spike feature occurs at the well documented phase transition to crystalline ice, and is another example of the "molecular volcano" [8].

Highly porous ice (Fig. 2c) shows a pair of distinct spikes in yield, the first occurring at 160 K,

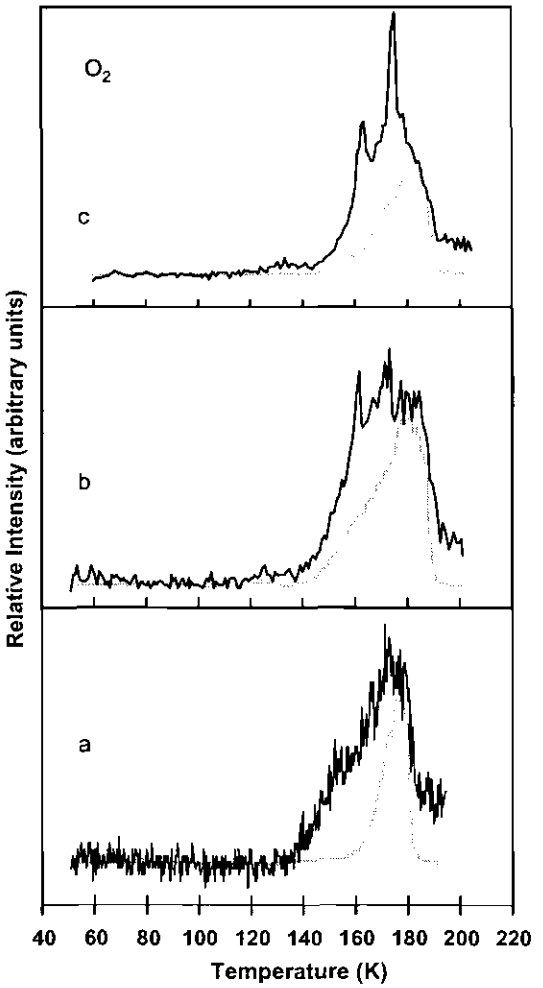

Fig. 2. Post-irradiation TPD of O_2 from (a) D_2O dosed at 150 K, (b) D_2O dosed at 120 K, and (c) D_2O dosed at 55 K. Irradiation of 100 eV electrons occurred at 55 K for all samples. For each curve, the corresponding TPD of the ice matrix is inset in the gray solid line (not to scale).

and another at 175 K. These both correspond to inflection points in the TPD of the ice. This second bump at higher temperature may be indicative of a gradual phase transition due to the poor thermal conductivity resulting from the presence of pores and the relatively slow heating rate (8 K/min).

Unlike D_2, O_2 is not released in the low temperature region below 120 K. This is well above the temperature of physisorbed O_2 on ice [9]. The effective radius of the oxygen molecule is much larger than that of D_2 and while D_2 is small enough to fit through the micropores of ice, O_2 may not be [6]. This would prevent O_2 from percolating through the ice matrix, while oxygen that is observed by ESD during irradiation, may originate in the near surface region close enough to escape into the vacuum. It may also escape through channels formed by radiation induced damage. Electron stimulated desorption of O_2 from low energy electrons on ice does not show a prompt component nor does it form from very thin (<2 ML) films [24,26]. Since production of O_2 requires a bimolecular mechanism to provide both oxygen atoms, it is likely that the mechanism is mediated by D-type Bjerrum defects which exhibit favorable orientation of adjacent water molecules for reactive scattering of oxygen atoms. This limits the locality of production to highly defect laden areas such as pore interfaces or grain boundaries.

There is no observed release of O_2 from PASW at 88 K, where D_2 shows a pronounced spike. If O_2 is trapped within the macropores, it is at a level below our detection limit. This is reasonable since the total ESD yield of O_2 at the temperature of irradiation of the sample (55 K) is at least 10 times smaller than D_2. Since O_2 is not formed directly at an interface, but just beneath it, and it does not effectively move through the microporous channels, the only O_2 that can reach the macropore is that which immediately surrounds it.

Previous measurements of the temperature dependence of the yield of O_2 by low energy electrons and high energy ions at low temperatures show striking similarity to that of D_2 [25,29]. With the exception of a hyperthermal direct component of D_2 that is independent of temperature [19], this correlation is interpreted as reflecting the temperature dependence of the electronic excitation mechanism responsible for the production of O_2 [25]. However, the transport mechanism responsible for bringing the O_2 product to the surface to be detected in ESD must be considered. O_2 and D_2 produced in the near surface region can escape without much loss due to trapping in pores. D_2 is known to be produced at the vacuum interface by a unimolecular dissociation channel that produces hyperthermal ejecta, whereas O_2 is produced in the near surface region. For PASW and ASW,

oxygen may be produced deeper within the ice film, either at defect sites or near the substrate/ice interface as was seen for D_2, [20,26] but cannot escape during ESD due to trapping. Finally, the energy required for production of O_2 may be transported into the film deeper than the penetration depth of low energy electrons. High energy ion bombardment is known to create damage tracks in ice due to momentum dominated scattering [30]. These tracks could allow for the escape of more O_2 during irradiation by releasing traps, and could account for some of the discrepancies in observed O_2 production by high energy ions vs low energy electrons at low temperature.

4. Conclusions

The effects of porosity and morphology of amorphous and crystalline D_2O ices on the electron stimulated generation and trapping of neutral molecular products D_2 and O_2, have been studied by post-irradiation thermal desorption. The trapped product yields increase from crystalline ice to amorphous ice to highly porous amorphous ice, similar to observed ESD yields. This can be attributed to the increased defect density of amorphous and highly porous amorphous ices. Low temperature release of D_2 in each case is associated with diffusion of D_2 through micropores in the ice matrix. Highly porous amorphous ice also shows a striking spike in the release of trapped D_2 at 80 K which has not previously been observed and must be a result of the presence of macropores. The trapped D_2 in macropores may result from transport of excitation energy to the enclosed volume interface resulting in direct dissociation. Molecular oxygen is not released in the same temperature range as D_2, but is retained within ice until much higher temperatures (140 K). This is attributed to sintering of grain boundaries and the release of clathrate hydrates in the lattice. Amorphous ice releases a burst of trapped O_2 at the 160 K amorphous to crystalline phase transition, which is consistent with previous codeposition experiments. Highly porous amorphous ice exhibits a much higher total yield of oxygen and shows an additional spike in trapped O_2 release at 175 K.

Acknowledgement

The authors gratefully acknowledge support from the NASA Office of Space Science, Planetary Atmospheres Program, grant no. NAG5-13234.

References

[1] P. Jenniskens, D.F. Blake, Science 265 (1994) 753.
[2] G.B. Hansen, T.B. McCord, J. Geophys. Res. [Planets] 109 (2004) E01012/1.
[3] T.L. Roush, J. Geophys. Res. [Planets] 106 (2001) 33315.
[4] D. Prialnik, A. Bar-Nun, Astrophys. J. 363 (1990) 274.
[5] G. Notesco, A. Bar-Nun, T. Owen, Icarus 162 (2003) 183.
[6] D. Laufer, E. Kochavi, A. Barnun, Phys. Rev. B 36 (1987) 9219.
[7] A. Bar-Nun, J. Dror, E. Kochavi, D. Laufer, Phys. Rev. B: Condens. Matter 35 (1987) 2427.
[8] K.P. Stevenson, G.A. Kimmel, Z. Dohnalek, R.S. Smith, B.D. Kay, Science 283 (1999) 1505.
[9] P. Ayotte, R.S. Smith, K.P. Stevenson, Z. Dohnalek, G.A. Kimmel, B.D. Kay, J. Geophys. Res. [Planets] 106 (2001) 33387.
[10] N. Horimoto, H.S. Kato, M. Kawai, J. Chem. Phys. 116 (2002) 4375.
[11] J.F. Cooper, R.E. Johnson, B.H. Mauk, H.B. Garrett, N. Gehrels, Icarus 149 (2001) 133.
[12] T.E. Madey, R.E. Johnson, T.M. Orlando, Surf. Sci. 500 (2002) 838.
[13] R.E. Johnson, Adv. Series Phys. Chem. 11 (2001) 390.
[14] M.T. Sieger, W.C. Simpson, T.M. Orlando, Nature 394 (1998) 554.
[15] I.G. Draganic, M.P. Ryan Jr., Z.D. Draganic, Adv. Space Res. 7 (1987) 13.
[16] V.I. Goldanskii, Nature 269 (1977) 583.
[17] N.G. Petrik, G.A. Kimmel, Phys. Rev. Lett. 90 (2003) 166102/1.
[18] T.M. Orlando, G.A. Kimmel, Surf. Sci. 390 (1997) 79.
[19] G.A. Kimmel, R.G. Tonkyn, T.M. Orlando, Nucl. Instrum. Methods Phys. Res. Sect. B 101 (1995) 179.
[20] N.G. Petrik, G.A. Kimmel, J. Chem. Phys. 121 (2004) 3736.
[21] T.M. Orlando, G.A. Kimmel, W.C. Simpson, Nucl. Instrum. Methods Phys. Res. Sect. B 157 (1999) 183.
[22] G.A. Kimmel, T.M. Orlando, Phys. Rev. Lett. 77 (1996) 3983.
[23] X. Pan, A.D. Bass, J.-P. Jay-Gerin, L. Sanche, Icarus 172 (2005) 521.
[24] T.M. Orlando, M.T. Sieger, Surf. Sci. 528 (2003) 1.
[25] R.E. Johnson, P.D. Cooper, T. Quickenden, G.A. Grieves, T.M. Orlando, J. Chem. Phys. in press.

[26] N.G. Petrik, G.A. Kimmel, J. Chem. Phys. 121 (2004) 3727.
[27] P.D. Cooper, R.E. Johnson, T.I. Quickenden, Planet. Space Sci. 51 (2003) 183.
[28] M.T. Sieger, T.M. Orlando. Surf. Sci. 451 (2000) 97.
[29] R.E. Johnson, Energetic Charged-Particle Interactions with Atmospheres and Surfaces, Springer-Verlag, Berlin, New York, 1990.
[30] R.E. Johnson, W.A. Jesser, Astrophys. J. 480 (1997) L79.

Available online at www.sciencedirect.com
SCIENCE DIRECT
ELSEVIER
Icarus 177 (2005) 528–533
ICARUS
www.elsevier.com/locate/icarus

The chemical nature of Europa surface material and the relation to a subsurface ocean

Thomas M. Orlando [a,b,*], Thomas B. McCord [c], Gregory A. Grieves [a]

[a] School of Chemistry and Biochemistry, Georgia Institute of Technology, 770 State St., Atlanta, GA 30332-0400, USA
[b] School of Physics, Georgia Institute of Technology, Atlanta, GA 30332, USA
[c] University of Hawaii, and Planetary Sciences Institute NW, P.O. Box 667, Winthrop, WA 98862, USA

Received 24 December 2004; revised 17 May 2005
Available online 6 July 2005

Abstract

The surface composition of Europa is of special interest due to the information it might provide regarding the presence of a subsurface ocean. One source of this information is the infrared reflectance spectrum. Certain surface regions of Europa exhibit distorted H_2O vibrational overtone bands in the 1.5 and 2.0 μm region, as measured by the Galileo mission Near Infrared Mapping Spectrometer (NIMS). These bands are clearly the result of highly concentrated solvated contaminants. However, two interpretations of their identity have been presented. One emphasizes hydrated salt minerals and the other sulfuric acid, although each does not specifically rule out some of the other. It has been pointed out that accurate chemical identification of the surface composition must depend on integrating spectral data with geochemical models, and information on the tenuous atmosphere sputtered from the surface. It is also extremely important to apply detailed chemistry when interpreting the spectral data, including knowledge of mineral dissolution chemistry and the subsequent optical signatures of ion solvation in low-temperature ice. We present studies of flash frozen acid and salt mixtures as Europa surface analogs and demonstrate that solvated protons, metal cations and inorganic anions all influence the spectra and must all, collectively, be considered when assigning Europa spectral features. These laboratory data show best correlation with NIMS Europa spectra for multi-component mixtures of sodium and magnesium bearing sulfate salts mixed with sulfuric acid. The data provide a concentration upper bound of 50-mol% for $MgSO_4$ and 40-mol% for Na_2SO_4. This newly reported higher sodium and proton content is consistent with low-temperature aqueous differentiation and hydrothermal processing of carbonaceous chondrite-forming materials during the formation and early evolution of Europa.

Keywords: Geochemistry; Ices; Satellites of Jupiter; Spectroscopy; Surfaces, Satellite

1. Introduction

Europa is the subject of intense scrutiny because of the possibility that its icy shell may conceal a liquid ocean capable of harboring life (Carr et al., 1998; Chyba, 2000; Chyba and Phillips, 2001). Evidence regarding crustal composition is limited, but includes sputtered atmospheric constituents (Brown, 2001; Brown and Hill, 1996; Hall et al., 1995) and near-infrared reflectance spectra of surface regions from the Galileo NIMS investigation (Carlson et al., 1996). Reflectance spectra of certain Europa surface regions exhibit highly distorted H_2O vibrational overtone bands. One interpretation is that these suggest endogenic frozen salt mineral mixtures with some Na_2SO_4 converted to H_2SO_4 under irradiation at the surface (McCord, 1998a; McCord et al., 1999, 2002). The other proposes that H_2SO_4 in ice gives the best single-component match to the NIMS spectra (Carlson et al., 1999). In the former, the salts come from the ocean below. In the latter, H_2SO_4 is from radiation processing and sulfur ion implantation in water ice from the jovian plasma torus. Hopes of accurate chemical identification of the surface material, and extrapolation to a

* Corresponding author. Fax: +1 404 894 7452.
E-mail address: thomas.orlando@chemistry.gatech.edu (T.M. Orlando).

0019-1035/$ see front matter
doi:10.1016/j.icarus.2005.05.009

subsurface ocean, will depend on integrating UV, visual and IR spectral data (Fanale et al., 1999), geochemical models (Kargel et al., 2000; Spaun and Head, 2001; Zolotov and Shock, 2001), and information on the tenuous and likely sputtered atmosphere (Johnson, 2000; Johnson et al., 2002; Leblanc et al., 2002) in a holistic view. However, interpretation of the reflectance spectra requires knowledge of mineral dissolution chemistry and the subsequent optical signatures of ion-solvation in low-temperature ice. All plausible models of Europa's formation and thermo-chemical evolution indicate that the crustal ice is not pure, but rather must contain some mineral content remnant of its formation from solar nebula solids.

Europa is a differentiated Moon-sized object, with a silicate core, water-rich mantle and ice crust that is subjected to strong energy input from Jupiter-induced tidal flexing (Carr et al., 1998; Geissler et al., 1998; Greeley et al., 2004; Khurana et al., 1998; Pappalardo et al., 1998). Thus, the layers beneath the icy crust could melt forming a liquid ocean which could foster the dissolution of core minerals. Though the thickness of the ice remains controversial, it is clear that it has been disrupted extensively from below. The materials present on the surface of Europa are the products of radiation transformations, cryovolcanism, impact and gardening events that have occurred over time. In fact, chemical alteration of the ice has been shown to produce condensed hydrogen peroxide within at least some icy surface regions (Carlson et al., 1999). Also, an atmosphere composed mostly of atomic and molecular hydrogen with some atomic and molecular oxygen from radiation processing of surface ice is seen (Hall et al., 1995; Orlando and Sieger, 2003; Sieger et al., 1998; Wu et al., 1978).

The chemical identity of the surface, when analyzed in conjunction with other mission data, can be considered as fingerprints of the past geochemical and geophysical activity. The association of the material with the disrupted regions on the surface strongly suggests an endogenic origin (McCord et al., 1998a, 1998b). Geochemical models suggest that salts such as $MgSO_4$ with Na_2SO_4 can be produced by low-temperature aqueous alteration of solar nebula material, as seen in carbonaceous chondrites (Kargel et al., 2000). This is expected to lead to the formation of Mg–Na–Ca-sulfate rich material, which, due to the presence of sulfidic base material, could also form some sulfuric acid (Kargel et al., 2000). Typically, salts in natural environments occur as mixtures, controlled by their source material, solubilities and formation temperatures. The relative abundances of these compounds depend upon the planetary condensation and internal Europa evolution temperatures, with lower temperatures favoring a relatively high sodium concentration. Some modeling has also been carried out which addresses the role of basic (Marion, 2001) and acidic conditions (Marion, 2002) on the freezing of aqueous solutions containing sodium and magnesium bearing sulfate salts.

The Galileo mission's Near Infrared Mapping Spectrometer (NIMS) returned infrared (IR) reflectance spectra (Carlson et al., 1996) exhibiting asymmetric absorption bands in the 1–3 μm spectral region (McCord et al., 1998a, 1998b). The primary features in this region are attributed to water ice overtones that shift in frequency and become asymmetric when ice contains certain types of impurities or when water molecules are in confined geometries. The asymmetric spectral signatures in the 1–3 μm region are concentrated on Europa in lineaments and chaotic terrain (McCord et al., 1998a, 1998b). We previously demonstrated that rapidly frozen brines give better spectral matches to the NIMS non-ice endmember spectrum than hydrous crystalline minerals (McCord et al., 2002). This rapid quenching/glass forming process preserves the water structures associated with the solvated ions in brine solutions. The complex cation, anion and proton solvation structures formed during flash freezing of aqueous solutions are possible sources of the perturbed optical signatures observed in the NIMS spectra. Thus, we undertook studies of flash frozen acid and salt mixtures as Europa surface analogs to examine the relative contribution of endogenic vs exogenic surface contamination.

2. Experimental

Infrared reflectance and temperature programmed dehydration were performed under low vacuum in a custom built chamber. The sample holder was a polished copper plate mounted to a rotatable flange which allows measurements to be taken both in diffuse and specular reflection. The sample mount was cooled with liquid nitrogen and resistively heated to achieve a temperature range of 77–400 K. Spectra were obtained using a Bruker Equinox 55 FTIR Spectrometer with an externally mounted detector (MCT, Infrared Associates Inc.). Infrared measurements were taken in diffuse reflection to more accurately base a comparison to the observational spectra from the Near Infrared Mapping Spectrometer aboard the Galileo spacecraft (McCord et al., 1998a, 1998b).

Salt solutions and acids were mixed in 1:8 mole ratio, with varying proportions of H^+, Na^+, and Mg^{2+} but constant SO_4^{2-} concentration. The samples were prepared by injecting saturated or highly concentrated acid or salt solution doses in multiple aliquots of small volume (10–25 μL) onto the cold sample surface through a septum port in the chamber. Previous experiments have made use of mixing a spectrally inert microcrystalline nucleus (diamond or SiO_2) to control grain size and limit optical penetration depth to obtain spectra comparable to those of NIMS (Carlson et al., 1999; Dalton, 2003). The spray technique utilized here produces a frosty texture that achieves equally acceptable spectral characteristics. The salts and acids used in this experiment were obtained from Aldrich and include $MgSO_4$, $MgCl_2$, Na_2SO_4, H_2SO_4, HNO_3, and HCl. Salt solutions were prepared at saturation at room temperature, while acids were mixed in 1:8 mole ratio with water. The solutions froze instantaneously on contact with the cold copper surface. De-

hydration was achieved by annealing the samples from the dosing point at 100 K up to a temperature adequate for water sublimation (~220 K) but below the crystallization point (>250 K) of the solutions. This is to simulate the long term erosion and thermal cycling of the surface of Europa in the vacuum of space. As a result of this dehydration step, the absolute concentrations of the salts in the ice are not known. All percentages reported here are in terms of mole fractions of the salts relative to each other.

3. Results and discussion

3.1. The relation of salt hydrolysis to acidity

Salt solutions, such as Earth's ocean, are generally considered to be of moderate pH since they are the result of acid–base neutralization reactions. For example, Na^+ is not capable of undergoing hydrolysis since it is the conjugate acid of a very strong base, thereby rendering it an extremely weak acid. However, cations such as Fe^{2+} and Mg^{2+} have large Z^2/r ratios (where Z is charge and r is the ionic radius) and therefore may react with water. Hydrolysis releases protons: i.e. $Mg^{2+} + H_2O \rightarrow MgOH^+ + H^+$. The proton is highly reactive and quickly forms a hydronium (H_3O^+) or Zundel cation ($H_5O_2^+$). The proton is also the primary product of the radiolysis of water ice. Although under terrestrial conditions, the hydrolysis of Mg^{2+}, released from the dissolution of $MgSO_4$, is counterbalanced by the weak nature of the second proton of sulfate, efficient ionization of HSO_4^- has been observed in low-temperature ice (Tomikawa and Hitoshi, 1998). The ionization probability was seen to increase exponentially with decreasing temperature, which should result in net release of solvated protons from magnesium hydrolysis over the temperature range typical of the Galilean satellite surfaces. This factor could provide a source term for a spectral signature of acids on an icy surface even if the contaminant material is endogenic in origin.

3.2. Infrared spectra of flash frozen salt and acid solutions

Fig. 1 shows a series of infrared spectra of flash frozen acids and salt brine solutions in the 1.4–2.6 μm region. For comparison, a NIMS non-ice endmember spectrum (McCord et al., 1999, 2002) is also shown. The spectra shown in Fig. 1 share a number of common features. Specifically, all spectra exhibit strong asymmetric peaks at 1.5 and 1.95 μm and most of the spectra have weak shoulder features at 1.58, 1.65, 1.80, and 2.2 μm. The feature at 1.65 mm is a distinct indicator of crystalline ice. The first three spectra are for flash frozen HNO_3, $MgCl_2$, and $MgSO_4$ and the following three are for flash frozen H_2SO_4, Na_2SO_4 and the NIMS spectrum. The position and width of the 1.95-μm feature of the NIMS spectra are reproduced well by all species containing sulfate anions. This feature can be associated with

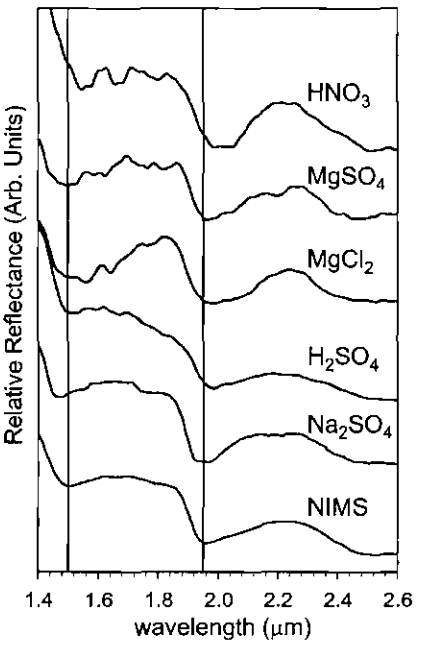

Fig. 1 Diffuse infrared reflectance spectra of selected flash frozen acids and salts. The bottom spectrum is the NIMS Europa non-ice endmember spectrum (McCord, 1998a, 1998b; McCord et al., 1999, 2002). Variations in the asymmetry of the 1.9–2.4 μm band are largely influenced by the nature of the anion–ice interaction, whereas bands in the 1.5–1.8 μm region are predominantly controlled by the cation and/or the presence of protons. Examining the role of both the cation and anion is critical in understanding these spectral signatures.

the $\nu_2 + \nu_3$ combination band of water, which is known to be perturbed by anions with diffuse charge distributions, such as SO_4^{2-} (Cannon et al., 1994). The perturbations on the hydrogen bonded network surrounding the anion are strong, resulting in a red-shift in stretch and a blue-shift in bend frequencies relative to bulk ice. Indeed, molecular dynamics simulations of the liquid phase indicate that the hydrogen atoms associated with the first solvation sphere are oriented toward the anion (Cannon et al., 1994). These average molecular arrangements are expected to be preserved during the flash freezing process. Singly charged anions, such as NO_3^- and Cl^-, show features close to that of the NIMS but careful inspection shows discernable and reproducible differences, particularly in the 2.2 and 2.09 μm shoulder features.

The asymmetric feature at 1.5 μm can be associated with the $\nu_1 + \nu_3$ combination band overtone of water and appears highly correlated with the presence of localized positive charge density. The spectra for material containing magnesium shows a very weak absorption at 1.80 μm, a feature clearly present in NIMS and the spectra for HNO_3, H_2SO_4, and Na_2SO_4. Thus, we associate the strong 1.80 μm feature as well as the induced asymmetry of the envelope between 1.5 and 1.8 μm primarily with the presence of protons and small cations such as Na^+. Although the hydrated proton is very mobile and ill defined in the liquid phase, it is immobilized in low-temperature ice (Cowin et al., 1999). The H^+

and Na^+ interact strongly with the surrounding water leading to polarization of the molecules and an elongation of the O–H bonds and the hydrogen bonding interactions between the first and second shells is increased. Calculations indicate (Lee et al., 2004) that the ion–oxygen distances are 2.3–2.4 Å for H^+ $(H_2O)_{n=1-6}$ and 2.4–2.5 Å for Na^+ $(H_2O)_{n=1-6}$. Thus, the overall structures and fundamental vibrational frequencies associated with these solvated cations are very similar (Bauschlicher et al., 1991). This is essential information that has not been taken into account when analyzing NIMS data on the distorted H_2O bands on Europa.

Fig. 1 also shows that the best *single-component* match to NIMS spectra is for H_2SO_4. Our spectrum is identical to that obtained by Carlson et al. (1999), using a diamond paste seeding method. The acids studied here are strong acids and are well-known sources of protons in aqueous solution and ice. Though it is tempting to suggest that acid mixtures are good surrogates for radiation-induced defects in ice, there are several significant discrepancies. Substitution of a water molecule by an acid molecule results in the increase of L-type orientational defects and hydronium ions, as well as concomitant reductions of D-type defects and hydroxyl ions (Takei and Maeno, 1987). The acid molecule also contributes its own fully solvated counter-anion, while radiation processed ice does not necessarily maintain charge neutrality. Thus, local defect configurations and equilibrium concentrations are not the same as those produced by incident radiation. Though H_2SO_4 produces a good, but not perfect, single component spectral match, we must consider multicomponent mixtures that might be better matches and that are more consistent with the inhomogeneous spatial distribution of the non-ice material and geochemical models.

3.3. *Infrared spectra of flash frozen salt and acid mixtures*

The compositions of several of the mixtures studied are presented in Table 1 and are relevant to those derived from models based on simple low-temperature aqueous dissolution of a primitive chondrite (Fanale et al., 2001; Kargel et al., 2000). Attempts to match the observed spectra by numerical weighted summing of lab spectra of pristine mineral samples (McCord et al., 1999) does not take into account nonlinear solute interactions with ionic strength, pH or limiting solvation volume, especially considering the degree of dehydration involved in these experiments. It is therefore necessary to actually mix these components together to make a valid assignment.

Table 1
Relative concentrations in mole-percent of constituents of flash frozen brine solutions that are models for the surface of Europa. Solution B can be equivalently made from $NaHSO_4$ rather than equal amounts of Na_2SO_4 and H_2SO_4

	$MgSO_4$	Na_2SO_4	H_2SO_4
A	0.50	0.10	0.40
B	0.50	0.25	0.25
C	0.70	0.15	0.15
D	0.33	0.33	0.33
E	0.24	0.40	0.35

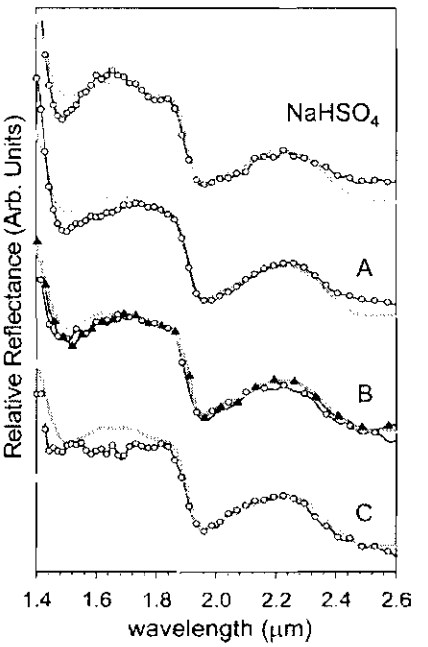

Fig. 2. Direct comparison of the diffuse reflectance spectra of selected flash frozen sulfate salt/acid mixtures to the NIMS data (gray line). The top spectrum is that of $NaHSO_4$. Spectrum A is a three component mixture containing 0.5:0.1:0.4 $MgSO_4$:Na_2SO_4:H_2SO_4, respectively. Spectrum B is of a solution with ratios 0.5:0.25:0.25 (open circles). Superimposed on spectrum B is the equivalent solution starting from $NaHSO_4$ rather than equal amounts Na_2SO_4 and H_2SO_4 (dark triangles). Frozen samples of the three component solutions give near perfect matches to NIMS data and clearly emphasize the role composites play in the surface composition of Europa. Each spectrum shows excellent agreement with the NIMS data in the 1.9–2.4 μm region as a result of the common sulfate anion. The spectrum labeled C containing 70 mole-percent $MgSO_4$ does not fit the NIMS data well. Solutions B and C also show good agreement with NIMS in the 2.5 μm region.

To examine the effect of sodium content, we flash froze $NaHSO_4$ and Na_2SO_4 solutions containing H_2SO_4. These mixtures may produce a similar chemical composition expected for radiation processed hydrated Na_2SO_4 (Carlson et al., 2002; Johnson et al., 2002; McCord et al., 2002). Plotted at the top of Fig. 2 is the spectrum of $NaHSO_4$ in direct comparison to the NIMS non-ice endmember spectrum (gray line). Also shown in Fig. 2 are spectra of $NaHSO_4$ and Na_2SO_4:H_2SO_4 solutions that contain various amounts of $MgSO_4$. The spectrum marked A (open circles) corresponds to a solution of 50% $MgSO_4$, 10% Na_2SO_4, and 40% H_2SO_4. This magnesium-rich solution has a noticeably increased absorption at 1.6 μm relative to that for the $NaHSO_4$ spectrum above, however the absorption at 1.5 μm is still too strong compared to NIMS. There are two spectra labeled B; one created from a mixture of $MgSO_4$ and $NaHSO_4$ (open circles), the other an equivalent mixture of $MgSO_4$ with equal amounts Na_2SO_4 and H_2SO_4 (filled triangles). The spectra are in excellent agreement with each

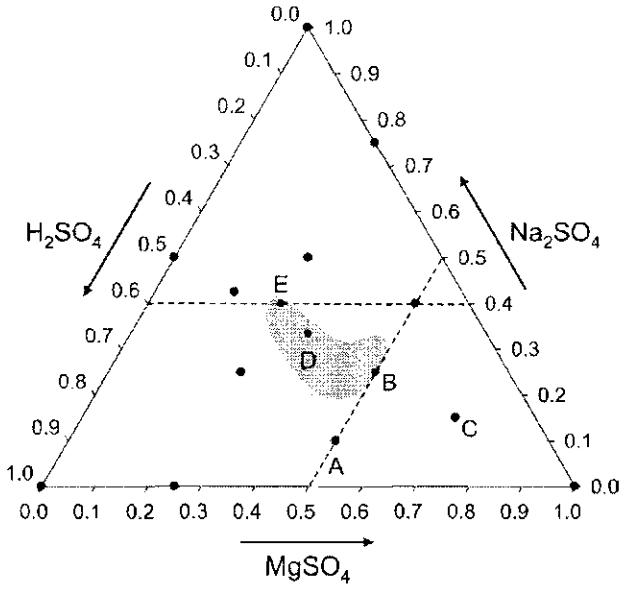

Fig. 3. Three-component diagram that brackets the relative concentrations of H_2SO_4, Na_2SO_4, and $MgSO_4$ that is likely present on the surface of Europa. The relative positions are determined from the laboratory concentrations and the gray zone delineates the best fits to the NIMS data. The best spectral matches occur for points B, D, and E. In general, a reasonable match is achieved when the amount of $NaSO_4$ is as high as 40 mol%, whereas the $MgSO_4$ cannot exceed 50 mol% (as indicated by dashed lines). Assuming this material is from an endogenous source, this information can be used to bracket the geochemical models on the evolution of the planet interior.

other, indicating that the flash freezing process traps the system in its fully dissolved state. Spectrum C is rich in $MgSO_4$ and matches poorly, whereas there is a near perfect spectral match for mixtures B, D, and E to the NIMS data.

3.4. Comparison of results to astronomical observation

In Fig. 3 is plotted a three-component diagram for the relative mole fraction of ternary mixtures of $MgSO_4$, Na_2SO_4, and H_2SO_4, assuming the presence of the minimum number of solvation waters. This diagram contains a summary of the lab spectra obtained and, with the exception of pure H_2SO_4, no single component spectrum is a reasonable match. The quality of fit was determined by the match of the band intensities and widths for each of eight spectral features located at 1.5, 1.58, 1.65, 1.80, 1.96, 2.09, 2.1, and 2.2 μm. The best fits to the NIMS non-ice material spectrum, which are contained within the gray region in Fig. 3, should be indicative of the relative concentrations of $MgSO_4$, $NaSO_4$, and H_2SO_4 in the Europa non-ice material. It should be noted that the relative amount of water is very small due to the annealing process and should be appropriate for comparing the NIMS non-ice endmember spectra. The correlation between the spectral features and the cation concentration from our data places upper limit concentrations of 50 mol% $MgSO_4$ and 40 mol% Na_2SO_4 for Europa non-ice material. This high Na_2SO_4 content is predicted in models of Europa with a relatively warm ocean and thin crust (Kargel et al., 2000). It is also consistent with the notion that sputtering of sodium-bearing salts is the source term for at least some of the Na observed in the tenuous atmosphere (Johnson et al., 2002; McCord et al., 2002). It is clear from these data that the presence of solvated protons is a necessary but not sufficient condition for interpreting the NIMS data.

The persistent presence of these sulfate minerals depends upon their thermal and radiation stability as well as the flux into or away from the surface. Dehydration of $MgSO_4$ and Na_2SO_4 minerals does not occur on a time frame less than several million years at average Europa surface temperatures and pressures (McCord et al., 2001). The sulfate ions and the associated waters of hydration are also quite stable to ionizing radiation (McCord et al., 2001). Radiation processing of frozen brines involves charge-transfer electronic transitions, which can neutralize a nearby Na^+, leading to the desorption of neutral atomic sodium with a non-thermal velocity distribution (Yakshinskiy and Madey, 1999), as observed by emission spectroscopy of the Europa atmosphere (Brown and Hill, 1996). Sputtering or electronic removal of neutral Mg from frozen $MgSO_4$ solutions is inefficient, since it is present as a solvated Mg^{2+} or $MgOH^+$ entity.

4. Conclusions

In summary, the NIMS reflectance spectral data of the Europa non-ice regions can be interpreted well in terms of the simultaneous existence of trapped protons and solvated Na^+, Mg^{2+}, and SO_4^{2-} ions. The source of the 1–3 μm spectral perturbations in ice are due to the geometric and electrostatic reorganization of the local hydrogen bonding networks associated with ion-solvation. Our results show that H^+, Na^+, and Mg^{2+} have characteristic effects on the spectral profile in the 1.5 μm band that can be used to estimate relative proportions thereof. Surface acidity is indicated by these results, and its presence is in addition to, not exclusive of, the presence of other salt cations from an endogenic source. Thus, although radiolysis of the europan surface must generate trapped protons, low-temperature ion hydrolysis will also contribute significantly to the acidity. The relative concentration of Na^+ suggested by our observations is higher than previous studies indicated. Comparing this to geochemical models of Europa formation implies a relatively cold condensation from primitive remnant chondrites (Kargel et al., 2000).

A europan surface composed of frozen mixed salt brines is the most consistent explanation of all available data. This includes (i) existing geochemical models, (ii) the distribution of non-ice spectra in the disrupted regions and along linea, (iii) the observed radiation-induced sputtering of neutral Na, and (iv) the observed ultraviolet absorption bands consistent with the presence of an oxide of sulfur. This interpretation bridges previous conflicting interpretations, as pointed out earlier on less evidence (McCord et al., 2002),

and helps provide a generally useful paradigm for assigning future spectra.

Since solvated ions can have very large effects on the dielectric properties of the hydration water molecules, techniques that are sensitive to variations in the dielectric properties, such as terahertz spectroscopy or radar, should be developed for future missions to Europa. The chemical and physical effects of high ion content on ice also suggests that studies of the electron, ion and photon radiolysis of ice will also be strongly influenced by salt contamination.

Acknowledgments

The authors acknowledge support from the NASA Office of Space Science, Planetary Atmospheres Program, grant No. NAG5-13234, and the Cosmochemistry Program, grant No. NAG5-10514.

References

Bauschlicher Jr., C.W., Langhoff, S.R., Partridge, H., Rice, J.E., Komornicki, A., 1991. A theoretical study of sodium(1+)-aqua complexes $(Na(H_2O)^+_{n=1-4})$. J. Chem. Phys. 95, 5142–5148.

Brown, M.E., 2001. Potassium in Europa's atmosphere. Icarus 151, 190–195.

Brown, M.E., Hill, R.E., 1996. Discovery of an extended sodium atmosphere around Europa. Nature 380, 229–231.

Cannon, W.R., Montgomery-Pettitt, B., McCammon, J.A., 1994. Sulfate anion in water—Model structural, thermodynamic, and dynamic properties. J. Phys. Chem. 98, 6225–6230.

Carlson, R., 24 colleagues, 1996. Near-infrared spectroscopy and spectral mapping of Jupiter and the Galilean satellites: Results from Galileo's initial orbit. Science 274, 385–388.

Carlson, R.W., Anderson, M.S., Johnson, R.E., Schulman, M.B., Yavrouian, A.H., 2002. Sulfuric acid production on Europa: The radiolysis of sulfur in water ice. Icarus 157, 456–463.

Carlson, R.W., 13 colleagues, 1999. Hydrogen peroxide on the surface of Europa. Science 283, 2062–2064.

Carlson, R.W., Johnson, R.E., Anderson, M.S., 1999. Sulfuric acid on Europa and the radiolytic sulfur cycle. Science 286, 97–99.

Carr, M.H., 21 colleague, 1998. Evidence for a subsurface ocean on Europa. Nature 391, 363–365.

Chyba, C.F., 2000. Energy for microbial life on Europa. Nature 406, 368.

Chyba, C.F., Phillips, C.B., 2001. Possible ecosystems and the search for life on Europa. Proc. Natl. Acad. Sci. USA 98, 801–804.

Cowin, J.P., Tsekouras, A.A., Iedema, M.J., Wu, K., Ellison, G.B., 1999. Immobility of protons in ice from 30 to 190 K. Nature 398, 405–407.

Dalton, J.B., 2003. Spectral behavior of hydrated sulfate salts: Implications for Europa mission spectrometer design. Astrobiology 3, 771–784.

Fanale, F.P., 24 colleagues, 1999. Galileo's Multiinstrument Spectral View of Europa's Surface Composition. Icarus 139, 179–188.

Fanale, F.P., Li, Y.H., De Carlo, E., Farley, C., Sharma, S.K., Horton, K., Granahan, J.C., 2001. An experimental estimate of Europa's "ocean" composition independent of Galileo orbital remote sensing. J. Geophys. Res.-Planets 106, 14595–14600.

Geissler, P.E., 14 colleagues, 1998. Evidence for non-synchronous rotation of Europa Galileo Imaging Team. Nature 391, 368–370.

Greeley, R., Chyba, C., Head, J.W., McCord, T.B., McKinnon, W.B., Pappalardo, R.T., Figueredo, P., 2004. Geology of Europa. In: Bagenal, F., Dowling, T., McKinnon, W. (Eds.), Jupiter: The Planet, Satellites and Magnetosphere. Cambridge Univ. Press, Cambridge, UK, pp. 329–362.

Hall, D.T., Strobel, D.F., Feldman, P.D., McGrath, M.A., Weaver, H.A., 1995. Detection of an oxygen atmosphere on Jupiter's moon Europa. Nature 373, 677–679.

Johnson, R.E., 2000. Sodium at Europa. Icarus 143, 429–433.

Johnson, R.E., Leblanc, F., Yakshinskiy, B.V., Madey, T.E., 2002. Energy distributions for desorption of sodium and potassium from ice: The Na/K ratio at Europa. Icarus 156, 136–142.

Kargel, J.S., Kaye, J.Z., Head III, J.W., Marion, G.M., Sassen, R., Crowley, J.K., Ballesteros, O.P., Grant, S.A., Hogenboom, D.L., 2000. Europa's crust and ocean: Origin, composition, and the prospects for life. Icarus 148, 226–265.

Khurana, K.K., Kivelson, M.G., Stevenson, D.J., Schubert, G., Russell, C.T., Walker, R.J., Polanskey, C., 1998. Induced magnetic fields as evidence for subsurface oceans in Europa and Callisto. Nature 395, 777–780.

Leblanc, F., Johnson, R.E., Brown, M.E., 2002. Europa's sodium atmosphere: An ocean source? Icarus 159, 132–144.

Lee, H.M., Tarakeshwar, P., Park, J., Kolaski, M.R., Yoon, Y.J., Yi, H.-B., Kim, W.Y., Kim, K.S., 2004. Insights into the structures, energetics, and vibrations of monovalent cation-(water)1–6 clusters. J. Phys. Chem. A 108, 2949–2958.

Marion, G.M., 2001. Carbonate mineral solubility at low temperatures in the Na–K–Mg–Ca–H–Cl–OH–HCO_3–CO_3–CO_2–H_2O system. Geochim. Cosmochim. Acta 65, 1883–1986.

Marion, G.M., 2002. A molal-based model for strong acid chemistry at low temperatures (<200 to 298 K). Geochim. Cosmochim. Acta 66, 2499–2516.

McCord, T.B., 11 colleagues, 1998a. Non-water–ice constituents in the surface material of the icy Galilean satellites from the Galileo near-infrared mapping spectrometer investigation. J. Geophys. Res.-Planets 103, 8603–8626.

McCord, T.B., 12 colleagues, 1998b. Salts on Europa's surface detected by Galileo's near infrared mapping spectrometer. Science 280, 1242–1245.

McCord, T.B., 11 colleagues, 1999. Hydrated salt minerals on Europa's surface from the Galileo near-infrared mapping spectrometer (NIMS) investigation. J. Geophys. Res.-Planets 104, 11827–11851.

McCord, T.B., Orlando, T.M., Teeter, G., Hansen, G.B., Sieger, M.T., Petrik, N.G., Van Keulen, L., 2001. Thermal and radiation stability of the hydrated salt minerals epsomite, mirabilite, and natron under Europa environmental conditions. J. Geophys. Res.-Planets 106, 3311–3319.

McCord, T.B., Teeter, G., Hansen, G.B., Sieger, M.T., Orlando, T.M., 2002. Brines exposed to Europa surface conditions. J. Geophys. Res.-Planets 107, 4/1–4/6.

Orlando, T.M., Sieger, M.T., 2003. The role of electron-stimulated production of O_2 from water ice in the radiation processing of outer Solar System surfaces. Surf. Sci. 528, 1–7.

Pappalardo, R.T., 10 colleagues, 1998. Geological evidence for solid-state convection in Europa's ice shell. Nature 391, 365–368.

Sieger, M.T., Simpson, W.C., Orlando, T.M., 1998. Production of O_2 on icy satellites by electronic excitation of low-temperature water ice. Nature 394, 554–556.

Spaun, N.A., Head, J.W., 2001. A model of Europa's crustal structure: Recent Galileo results and implications for an ocean. J. Geophys. Res.-Planets 106, 7567–7576.

Takei, I., Maeno, N., 1987. Electric characteristics of point defects in hydrogen chloride-doped ice. J. Phys. Colloq. 48/3, C121–C126.

Tomikawa, K., Hitoshi, K., 1998. Raman study of sulfuric acid at low temperatures. J. Phys. Chem. A 102, 6082–6088.

Wu, F.M., Judge, D.L., Carlson, R.W., 1978. Europa: Ultraviolet emissions and the possibility of atomic oxygen and hydrogen clouds. Astrophys. J. 225, 325–334.

Yakshinskiy, B.V., Madey, T.E., 1999. Photon-stimulated desorption as a substantial source of sodium in the lunar atmosphere. Nature 400, 642–644.

Zolotov, M.Y., Shock, E.L., 2001. Composition and stability of salts on the surface of Europa and their oceanic origin. J. Geophys. Res.-Planets 106, 32815–32827.

Production of oxygen by electronically induced dissociations in ice

R. E. Johnson
Engineering Physics, Thornton Hall B103, University of Virginia, Charlottesville, VA 22904

P. D. Cooper and T. I. Quickenden
Chemistry M313, School of Biomedical and Chemical Sciences, The University of Western Australia, 35 Stirling Highway, Crawley, Western Australia 6009, Australia

G. A. Grieves
School of Chemistry and Biochemistry, Georgia Institute of Technology, Atlanta, Georgia 30332

T. M. Orlando[a)]
School of Chemistry and Biochemistry, Georgia Institute of Technology, Atlanta, Georgia 30332 and School of Physics, Georgia Institute of Technology, Atlanta, Georgia 30332

(Received 4 March 2005; accepted 9 September 2005; published online 9 November 2005)

A solid-state chemical model is given for the production of O_2 by electronic excitation of ice, a process that occurs on icy bodies in the outer solar system. Based on a review of the relevant available laboratory data, we propose that a trapped oxygen atom-water complex is the principal precursor for the formation of molecular oxygen in low-temperature ice at low fluences. Oxygen formation then occurs through direct excitation of this complex or by its reaction with a freshly produced, nonthermal O from an another excitation event. We describe a model for the latter process that includes competition with precursor destruction and the effect of sample structure. This allows us to put the ultraviolet photon, low-energy electron, and fast-ion experiments on a common footing for the first time. The formation of the trapped oxygen atom precursor is favored by the preferential loss of molecular hydrogen and is quenched by reactions with mobile H. The presence of impurity scavengers can limit the trapping of O, leading to the formation of oxygen-rich molecules in ice. Rate equations that include these reactions are given and integrated to obtain an analytic approximation for describing the experimental results on the production and loss of molecular oxygen from ice samples. In the proposed model, the loss rate varies, roughly, inversely with solid-state defect density at low temperatures, leading to a yield that increases with increasing temperature as observed. Cross sections obtained from fits of the model to laboratory data are evaluated in light of the proposed solid-state chemistry. © *2005 American Institute of Physics*.
[DOI: 10.1063/1.2107447]

I. INTRODUCTION

Oxygen has been detected in the very thin atmospheres on the icy moons of Jupiter, and peroxide and oxygen-rich molecules have been observed as trapped species in their icy surfaces. The observed O_2 is primarily a product of the decomposition of ice by energetic ions and electrons trapped in the Jovian magnetosphere.[1–4] More recently molecular oxygen ions have been detected over the rings of Saturn suggestive of an oxygen ring atmosphere produced by ultraviolet (UV) photon-induced production of O_2 in ice.[5] In addition, molecular oxygen, hydrogen peroxide, and oxidized sulfur and carbon have all been detected as trapped species *in* the icy satellite surfaces.[4,6] At the icy moon Europa, the proposed transport of these oxygen-rich species to its putative subsurface ocean as a means of sustaining aerobic life processes[7] has excited the astrophysical community. This has also motivated us to describe the solid-state chemistry that follows the production of electronic excitations in ice.

In this paper, we summarize the laboratory database for radiation-induced production of O_2 from ice. We then use these results as a guide in describing the physical and chemical processes leading to the formation of molecular oxygen by energetic charged particles (e.g., ions), electrons, and ultraviolet (UV) photons incident on an ice sample. Our goal is to characterize the primary physical and chemical pathways for the nonthermal production of oxygen in low-temperature ice. Quite remarkably, a quantitative model for this was not available in spite of laboratory studies that have been carried out since the 1950s. Thus, we give a model for the chemical pathways at low doses that differs from those models typically suggested to be dominant in water. We show that the model is consistent with available data and suggest critical experimental tests.

Following a brief review of the space observations, we summarize the principal results of the considerable laboratory data on the radiolysis and photolysis of ice in order to motivate the model. We then describe the generalized rate equations for a chemical kinetic model for production of molecular oxygen in ice. In this model, trapping at defects and percolation from depth play important roles. These equations are then integrated over the depth of penetration of the

a)Author to whom correspondence should be addressed. Electronic mail: thomas.orlando@chemistry.gatech.edu

radiation and simplified to obtain an approximate analytic expression for the yield of molecular oxygen from ice that can be tested experimentally. This expression also reduces to the precursor model of Sieger *et al.*[2] and Orlando and Sieger.[3] Fits of the model to the available data are used to extract primary dissociation and reaction cross sections and to show the commonality of the results for photon, electron, and fast-ion-induced chemistry. We also show that hydrogen peroxide (H_2O_2) or the superoxide (HO_2) are not necessary precursors for oxygen production from a fresh ice sample, although they likely become important at higher doses and on annealing of the irradiated samples.[8]

II. SUMMARY OF SPACE OBSERVATIONS AND LABORATORY STUDIES

Gas-phase oxygen has been observed to be associated with the icy bodies in the Jovian and Saturnian systems as discussed.[4] In addition, two well-known transitions for interacting pairs of O_2 molecules at 577.2 and 627.5 nm were observed in the reflectance spectra of Jupiter's moons Ganymede[9] and Europa.[10] These bands are associated with the O_2 dimer,[11] suggesting that molecular oxygen is locally dense, likely as an inclusion in the icy surface.[9,12] Finally, the Hartley band of O_3 has been tentatively identified in the UV absorption spectra of certain icy satellites.[13] Although the band shape suggests that additional absorbing species are present,[14] O_3 trapped within the icy surface is consistent with the presence of trapped oxygen inclusions exposed to radiation.[1,12] This feature is superimposed on a broad UV absorption extending from about 0.4 μm to shorter wavelengths and attributed to another radiolytically produced oxidant, H_2O_2, which was also identified in the infrared (IR).[15] Consistent with the above, oxygen-rich molecules appear to be produced by the radiation processing of ice containing sulfur
(SO_2 and a sulfate) and carbon (CO_2 and a carbonate).[6] Below we summarize the laboratory data bases showing a few of the principal results.

Although impurities are known to affect luminescence in ice,[16] the production of O_2 by *photolysis* was inferred via luminescence from thick samples of ice formed from purified water.[17] In most other studies, the radiation-induced production of O_2 from ice is detected in the gas phase by a quadrupole mass spectrometer (QMS) either after warming or during irradiation as an outgassed species. In the latter experiments, the production efficiency is given as a yield, the number of O_2 produced during irradiation of the sample per electron, ion, or photon incident. This is a quantity we will calculate below. In such studies, the O_2 that remains trapped in the ice is typically not measured.

Though some early radiolysis experiments were likely affected by impurities, the ion- and electron-beam results presented in this paper were carried out in ultrahigh vacuum (UHV) with very pure ice samples. Though the techniques have been described in detail, we present a brief description of the most relevant facts concerning the low-energy electron experiments.[2,3] Briefly, an UHV chamber (base pressure of 1×10^{-10} Torr) was equipped with a pulsed low-energy (5–250 eV) electron gun, a cryogenically cooled sample holder, and a QMS. The electron beam has a maximum time-averaged current density of $\sim10^{14}$ electrons/cm^2 s and a typical beam spot size of $\sim$1.5 mm. The maximum total dose used in the experiments reported here is $\sim10^{15}$ electrons/cm^2 which was achieved using pulsed irradiation over a 100 s interval. The typical pulse width was 100 μs and the frequency used was 1000 Hz. The current density per pulse never exceeded $\sim10^{10}$ electrons/cm^2 pulse. This is an effective impingement rate of one low-energy electron per 10^5 surface molecules. Even after limited phonon excitation and secondary scattering, the subsequent heating of the surface during our pulsed electron-beam dosing condition is negligible. Since there is a secondary-emission yield from ice and holes at the surface are not all neutralized by recombination,[18] measurable surface charging occurs rapidly.[19] A quasisteady state is reached at doses as low as $\sim10^{13}$ electrons/cm^2, and then the surface charge changes very slowly. Therefore, charging cannot account for the principal fluence dependence observed for the O_2 yield.

Ice thin films were grown after several freeze-pump-thaw cycles by controlled vapor deposition on either Pt(111) or graphite substrates. Note that oxygen was never observed/present in the absence of radiation. The substrates were heated resistively which allowed for temperature control from 80 to 500 K. The substrate temperature was monitored with a thermocouple and a computer-controlled feedback system drove the temperature ramp at a rate of 8 K/min. Porous amorphous solid water (PASW) samples were deposited at 80 K with a directional doser oriented approximately 70° from normal incidence. Nonporous amorphous solid water (ASW) samples were dosed between 110–120 K at normal incidence and crystalline ice (CI) samples were deposited between 150 and 155 K. Film thickness is estimated to be between 50–100 ML by comparison to published temperature-programmed desorption data.

The principal dissociation processes in ice lead to H, OH, H_2, and O, but the principal species that escape from an irradiated ice sample are those that have the lowest binding energies to ice: H_2, O_2, and H_2O. That is, surface binding and reactive pathways act as filters for the ejecta. Therefore, gas-phase O_2 coming from an irradiated sample in a vacuum can be readily detected although decomposition of bulk ice is inefficient.

At low doses the O_2 yield was found to increase linearly with dose until saturation occurs. This dependence has been seen in a number of experiments and is shown in Figs. 1(a) and 1(b) for a fast heavy ion and low-energy electrons. These yields have also been shown to be temperature dependent by a number of laboratories using several types of incident radiation. As an example, this is shown at saturation for incident 1.5 MeV Ne^+ and low-energy electrons in Figs. 2(a) and 2(b). For temperatures $<\sim140$ K, the yield of O_2 and D_2 produced from vapor-deposited ice samples at low radiation doses decreases with decreasing temperature. It has been shown repeatedly, over most of the temperature range studied, that the measured yields depend on the total dose and not the dose rate, although this has *not* been tested at the higher temperatures shown in Figs. 1 and 2. Also seen in Fig. 2(b) is a clear drop in the yield for temperatures above

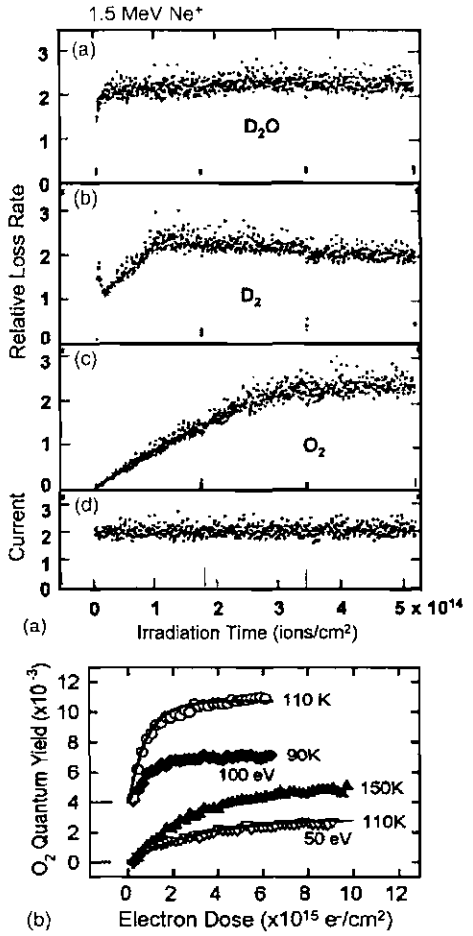

FIG. 1. (a) Relative yields vs fluence (ion flux × time) for 1.5 MeV Ne^+ incident on D_2O ice at 7 K (adapted from Reimann *et al.* 1984) (Ref. 21). Top panel: DxO yield. Middle panel: D_2 yield. Bottom panel: O_2 yields. Yields at other temperatures exhibited similar dependences with the slope of O_2 yield vs fluence varying with T. Fit to the O_2 yield gives parameters in Table I and fits to temperature dependence give activation energies between ~0.02 eV at the lowest fluences and lowest T to ~0.07 eV at the highest T and highest fluences. (b) Yield of O_2 vs fluence of low-energy electrons on D_2O ice for two electron energies and a number of temperatures (from Sieger *et al.*, 1998) (Ref. 2). The lines through the data are the fits using Eq. (4a) in this text. The fits were used to extract the parameters for low-energy electrons given in Table I.

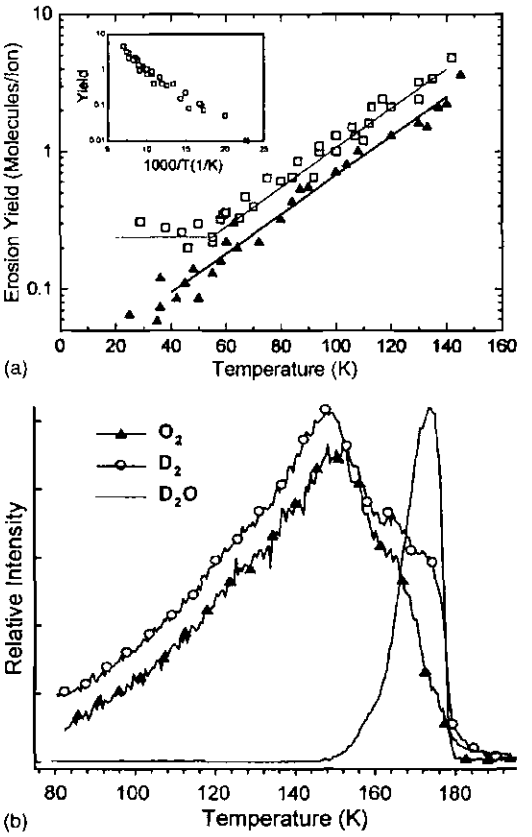

FIG. 2. (a) Yield for D_2 and O_2 at saturation (steady state) from 1.5 MeV He^+ on D_2O ice vs the temperature of the ice (adapted from Brown *et al.*, 1982) (Ref. 39). Inset: D_2 yield minus the constant yield at low T vs $1/kT$, giving an activation energy of ~0.03 eV. (b) Yield for O_2 and D_2 vs temperature for incident electrons at saturation (steady state), showing the correlation between the production of D_2 and O_2 in steady state. Also shown is the sublimation of the D_2O sample that occurs at the higher temperatures. Note the amorphous to cubic phase transition occurs between 145 and 160 K.

150 K. This drop has been shown to be related to the amorphous to cubic phase transition which is manifested by the small shoulder on the leading edge of the thermal desorption yield (solid line with no symbols) of molecular water.[3] There is also a shoulder prominent in the D_2 yield at 170 K that is due to reactive scattering in the gas phase.

The O_2 yields have also been shown to depend on the sample formation temperature and crystal state,[3] indicating that structure and defects can affect the O_2 yield. An O_2 production "threshold" of ~5.3 eV was suggested by the photolysis experiments of Mattich *et al.*[17] In the UHV experiments a threshold of ~6.5 eV (cross section $\sim 10^{-20}$ cm^2) was found using low-energy electrons[2,4] with a similar threshold for O (^4P, ^1D) and H_2 productions.[20] As seen in Fig. 1(a), D_2 is promptly ejected from D_2O ice whereas O_2 is not. However, after an incubation dose, the O_2 yield and D_2 yields in steady state are correlated,[21,22] as indicated in Figs. 2(a) and 2(b). In this way the stochiometry of the surface layer is only slightly altered.[23]

The temperature dependencies for the yield of O_2 from ice have been repeatedly interpreted in terms of effective activation energies. At temperatures ~40–120 K, these were found to be relatively small (~0.03 eV) [Fig. 2(a)]. Such energies are equivalent in size to activation energies for mobility of protons or hydrogen in ice and for structural rearrangements. Finally, for thin samples and penetrating radiation, percolation of oxygen from depth can occur so that the yields are found to depend on the sample thickness. Since the measured yields were also shown to depend on the excitation density, sample formation, and temperature, comparisons between experiments have proven to be difficult.

Hydrogen peroxide and related species formed by incident radiation are not readily ejected into the gas phase, but can be detected via absorption bands as trapped species in an irradiated ice sample.[24–26] Hydrogen peroxide forms via the principal dissociation product, OH, and the production yields correlate with H_2 formation.[4] Hydrogen peroxide and/or HO_2 have been suggested[7] as potential precursor species for the

formation of O_2. However, the fluence dependence observed in the QMS experiments suggests that O_2 can be formed by a process that does not involve these species, as describe below. In addition, recent matrix isolation studies indicate that trapped O can be converted to hydrogen peroxide and hydrogen peroxide converted into trapped O by incident radiation (i.e., H_2O $O+h\nu \rightarrow H_2O_2$; $H_2O_2+h\nu \rightarrow H_2O+O$).[27] In the model below, trapped O is the principal species considered for formation of O_2 at low doses. At higher doses, the conversion of hydrogen peroxide to trapped O can provide additional channels for O_2 formation that may involve[8,28] pairs of H_2O_2 or HO_2. Although on a planetary surface the high-dose results may be more relevant, here we are primarily interested in the new channel occurring at relatively low doses in order to interpret a number of recent laboratory results. Below we construct a chemical kinetic model of the production of O_2 and then use this model to interpret a number of experiments.

III. MODEL FOR FORMATION OF O_2

The yield of O_2 from ice at low temperature increases linearly with radiation fluence (flux × time or dose) at the low fluences as indicated in Fig. 1 and is independent of beam flux. Quite remarkably, this is the case both for low-energy electrons that make a single excitation for each impact and fast ions that make a density of excitations along their path through the solid. At low temperatures, if the beam is turned off and later turned back on, the measured yield returns to the value it had before the beam was turned off indicating that a stable chemical alteration occurred.[2,21] Therefore, either the ice is chemically altered before the incident radiation produces O_2, or O_2 is produced and trapped in the solid and then caused to escape by the subsequent radiation. Whereas the former is the case for the low-energy electrons, both processes occur for penetrating radiation.[4] It is the preferential loss of hydrogen [e.g., Fig. 1(a)] from an irradiated ice that enhances the likelihood of forming oxygen-rich precursors and the subsequent production of molecular oxygen.[1-4] Therefore, we consider the chemical precursors and the production of O_2 during the irradiation of ice.

The analytic model used by Seiger *et al.*[2] to fit their electron data is first reviewed. This is followed by the more detailed chemical kinetic model for the radiation processing of ice at the low fluences shown in Fig. 1. This model is then used to obtain cross sections from the available laboratory data.

A. Analytic precursor model

In describing their electron irradiation experiments, Seiger *et al.*[2] separated the temperature-dependent precursor formation step from the temperature-independent O_2 production step. The column density of a precursor species N_p formed in ice by incident radiation was calculated using cross sections for production σ_p and destruction σ of the precursor. O_2 is then formed by direct or indirect electronic excitation of this precursor described by the cross section σ_{O_2}. The model is described by a pair of simple rate equations, one for N_p and one for the production rate of oxygen dN_{O_2}/dt,

$$dN_p/dt = \sigma_p \phi N - \sigma \phi N_p, \tag{1}$$

$$dN_{O_2}/dt = \sigma_{O_2} \phi N_p. \tag{2}$$

Here ϕ is the radiation flux and N is the column density of H_2O from which the incident radiation can produce and eject O_2. For low-energy electrons, N is a few monolayers ($\sim 3 \times 10^{15}$ H_2O/cm^2) but N is much larger for energetic ions. Here we write the destruction cross section as $\sigma = \sigma_p' + \sigma_{O_2}$ where σ_p' accounts for precursor destruction processes other than the formation of O_2.

Solving Eq. (1) assuming N is nearly constant, the fraction of precursors c_p in the penetrated column after time t is

$$c_p = N_p/N = [\sigma_p/\sigma][1 - \exp(-\sigma\Phi)]. \tag{3}$$

Here $\Phi = [\phi t]$ is the fluence (flux × time), the number of particles (photons, electrons, or ions) incident on the surface per unit area. Using c_p in Eq. (2), the O_2 yield Y at any fluence can be written in terms of the yield at steady state, Y_∞,

$$Y = [dN_{O_2}/dt]/\phi = \sigma_{O_2} c_p N = Y_\infty [1 - \exp(-\sigma\Phi)], \tag{4a}$$

$$Y_\infty = [\sigma_p \sigma_{O_2}/\sigma] N. \tag{4b}$$

Accounting for the destruction of water molecules in the initial column, N, changes the result in Eq. (4) only slightly. Photolysis experiments suggest that the number of dissociated water molecules in steady state is $\sim 10\%$ of the irradiated column.[29]

The form in Eq. (4a) gave excellent fits to the incident electron data,[2] as seen in Fig. 1(b). In order to extract *both* σ_p and σ_{O_2} from these fits to the yield versus fluence data, it was also assumed that the production of O_2 is the principal precursor destruction process, i.e., $\sigma \approx \sigma_{O_2}$ and $\sigma_p' = 0$. However, other precursor destruction processes can dominate σ, especially for penetrating radiation, as discussed below.

In the above model the precursor is formed in a single excitation event in a fresh ice sample. For low-energy ionizing radiation, hydrogen peroxide, a suggested precursor, is formed as a product of two dissociation events in ice,[25] i.e., $2H_2O \rightarrow 2H + 2OH \rightarrow H_2 + H_2O_2$. If it were the principal precursor, the form for the yield in Eq. (4a) could be roughly recovered. However, there would be an offset due to the two-step precursor formation process, i.e., $Y \approx Y_\infty[1 - \exp(-\sigma\Phi) - \Delta]$, where Δ is determined by the peroxide formation and destruction processes.[3] This would also be the case if our proposed precursor was formed in any other process that required two excitation events, such as $H_2O \rightarrow H + OH \rightarrow H + H + O$. Since no obvious offset at low fluences was observed, we consider a precursor formed by a single energy absorption event.

B. Trap density and trapped O

In Eqs. (1) and (2), the density of trapping sites n_t is not explicitly included. However, trapping sites and porosity have been shown to be important for ice chemistry.[17,21,30]

Although the density of defects, voids, and interfaces *decrease* as the formation temperature of the ice increases, the efficiency of production of O_2 is the opposite, increasing with increasing T for $T \leq \sim 140$ K.

We propose that trapped oxygen atoms are the principal precursor at low fluences. O_2 is then formed by the reaction of O (or OH) with this precursor or by electronic excitation of the precursor complex. Here we describe the kinetics of the production of O_2 by O-atom reactive scattering. This is similar to the production of CO_2 in a CO/H_2O ice mixture.[31] A paper describing the role of direct and indirect electronic excitations of the precursor is the subject of a separate paper.[22]

Following dissociation to H_2+O, which is given by the absorption cross section σ_d', H_2 is lost from the ice samples at the temperatures above ~40 K. The O produced by ions or electrons can be in the ground-state or in the excited singlet and triplet states. However, the UV absorption below the band gap can only produce excited singlet states. These can quench in the ice matrix releasing energy but eventually trap. The newly formed O produces an oxygen-water molecule complex, $O\cdots(H_2O)_n$, which we refer to in the following as trapped O, O_t. This occurs according to the reaction rate $k_{O,t}$, and we propose this as a precursor to the formation of O_2. This precursor might produce O_2 on excitation,[22] but here we suggest that a subsequent radiation absorption can again produce a nonthermal O via H_2+O (σ_d'). The nonthermal O can react with O_t within some reaction radius resulting in the formation of $O_2[O+O_t \rightarrow O_2]$ described by $k_{O,Ot}$. These two excitation events give a net production of two H_2 and an O_2.

The principal dissociation channel ($H_2O \rightarrow H+OH$), described by σ_d, produces a mobile H. It can also react with O_t, described by $k_{H,Ot}$, removing trapped O. Nonthermal H and O can also be removed by other reactants R [e.g., $R+H \rightarrow RH(k_{H,R}n_R)$; $R+O \rightarrow RO(k_{O,R}n_R)$, where R can be a radiation product, such as OH, or a contaminant in the ice]. Reaction of a newly formed, mobile and electronically excited OH with O_t might also produce O_2, a process that needs to be tested experimentally. We ignore this in the model and also initially ignore the conversion of trapped O to hydrogen peroxide by an electronic excitation.[4]

The principal reaction pathways considered for oxygen are

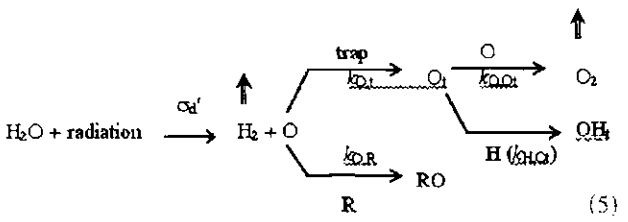

(5)

This leads to a set of rate equations:

$$dn_O/dt = \sigma_d'\phi n - k_{O,t}n_O n_t - k_{O,R}n_O n_R - k_{O,Ot}n_O n_{Ot}, \quad (6a)$$

$$dn_{Ot}/dt = k_{O,t}n_t n_O - k_{O,Ot}n_O n_{Ot} - k_{H,Ot}n_H n_{Ot}, \quad (6b)$$

$$dn_H/dt = \sigma_d\phi n - k_{H,Ot}n_H n_{Ot} - k_{H,R}n_H n_R, \quad (6c)$$

$$dn_{O_2}/dt = k_{O,Ot}n_O n_{Ot}. \quad (6d)$$

Here n_i is the density of species i in the irradiated volume and n_t is the density of trapping sites. As in Eq. (2), O_2 destruction processes are ignored in Eq. (6d), since for low-energy electrons the newly produced O_2 can escape from the excited near surface layers. For penetrating radiation this changes and O_2 that did not escape can, in principle, be dissociated by a subsequent excitation event. In addition, if direct excitation of the precursor can produce O_2, then the term $[k_{O,Ot}n_O n_{Ot}]$ in Eqs. (6a), (6b), and (6d) is replaced by a term like $\sigma_{O_2}\phi\, n_{Ot}$. The above equations act in parallel with the equations for formation of OH and hydrogen peroxide described elsewhere.[4]

Integrating the above equations over the depth of escape of O_2 from an irradiated sample, the analytic precursor model of Seiger *et al.*[2] is recovered.[4] Therefore, σ_p, σ_p', σ_{O_2} and σ can now be determined in terms of the rate constants and primary dissociation cross sections.

C. Trapped versus newly produced species

In the solid state the role of defects is critical. Defects are produced by sample formation at low-temperatures and, for penetrating radiation, defects/damage sites are produced by the irradiation itself. Since the newly produced species from an excitation event trap in times short compared to the time scale of the incident particle fluxes typically used, a steady-state background of nonthermal O does not accumulate. Therefore, the above equations can be solved simultaneously. That is, there are trapped O and freshly produced O that rapidly react or trap. If the density of traps is large, then the quantities n_H and n_t, averaged over the bombardment rate, are roughly time independent: $dn_O/dt \sim 0$ and $dn_H/dt \sim 0$. Therefore, only species trapped at defects, pores, or grain surfaces are assumed to be present before a subsequent impact. This is consistent with the lack of a dependence of the O_2 yield on the incident beam flux at those temperatures that have been tested for dose rate effects: <120 K. Solving Eqs. (6a) and (6c) for n_O and n_H, which describe the transiently mobile O and H, and substituting, Eqs. (6b) and (6d) reduce to the rate equations Eqs. (1) and (2) with O_t as the precursor.

Since the density of trapped O n_{Ot} is small compared with the density of sites at which H can react, then from Eq. (6c) $n_H \sim [\sigma_d\phi n/k_{H,R}n_R]$. For a low radiation flux ϕ, the average value of n_H is small. The O_2 yield Y_{O_2} is equal to $|(dn_{O_2}/dt)\Delta x/\phi|$ with Δx being the O_2 escape depth. The yield can now be written in the form given in Eq. (4a) with an analytic expression for the steady-state yield Y_∞,

$$[Y_\infty]/[\sigma_d'N] = 1 + \{(q-1) - [(q-1)^2 + 8q\delta]^{0.5}\}/4\delta,$$

$$q = [k_{O,t}(n_t + n_R)](k_{H,Ot}n_H)/(\sigma_d'\phi n)k_{O,Ot}$$
$$= (\sigma_d/\sigma_d')[k_{O,t}(n_t + n_R)]k_{H,Ot}/[k_{O,Ot}k_{H,R}n_R] \quad (7)$$

$$\delta = 0.5[1 + n_t/(n_t + n_R)].$$

We further note that for large n_t and small ϕ, q can be large Assuming that $q \gg 1$ and that $n_t \gg n_R$, then Eq. (7) becomes

$$Y_\infty \rightarrow [\sigma_d' N]/d \approx (\sigma_d'/\sigma_d)N\zeta,$$
$$\zeta \approx [(k_{O,O_t}k_{H,R})/(k_{H,O_t}k_{O,t})][n_R/n_t] \quad (8)$$

Here the factor ζ accounts for the competing reactions. The result in Eq. (8) is based on the fact that the production of H is more efficient than the production of O (i.e., $\sigma_d \gg \sigma_d'$ so that the destruction of the precursor, O_t, by reaction with H is more efficient than the reaction with mobile O to form O_2. Comparing Eq. (8) with the expression for Y_∞ in Eq. (4b), we can write $\sigma_p \sim \sigma_d'$, $\sigma_{O_2} \sim \sigma_d'$ and $\sigma \approx \sigma_p' \sim \sigma_d$. Since mobile H and O affect both the numerator and denominator of ζ, writing $k_i \approx [\sigma_i v]$, where the σ_i is an interaction cross section (square of an interaction length) and v_i the mean speed of the mobile species, the ratio $\zeta \approx [(\sigma_{O,O_t}\sigma_{H,R})/(\sigma_{H,O_t}\sigma_{O,t})] \times [n_R/n_t]$ is the ratio of interaction cross sections times the density of reaction sites to density of traps ratio. That is, the precursor destruction rate is proportional to the quenching of O_t by H, which occurs in competition with the loss of mobile H by other reactions including recombination to form H_2O. At saturation, the reaction sites are primarily dissociation products.

It is seen from Eq. (8) that the steady-state yield Y_∞ depends inversely on the density of traps n_t. That is, when the trap density is high, O_2 formation requires that a newly formed O find a trapped O before it becomes trapped or reacts with impurities or other radiation products. Therefore, the observed increase in the O_2 yield with increasing T at low doses is related to the change in the trapping density n_t with increasing temperature of the ice sample. In this model, the small activation energy measured (Fig. 2) is related to the reorientation of defects leading to a reduction in trap density. As the sample formation temperature increases and the density of traps in the bulk decreases, the surface and grain interfaces eventually become the dominant traps.[22,32] Radiation-induced defects/damage become important trapping sites for penetrating radiation and thus increases of dose can affect the production of molecular oxygen. In addition, O_2 production can increase in the presence of oxygen-rich impurities, such as CO_2 or SO_2, since their dissociation can also provide mobile O. Such species also act as hydrogen scavengers[26] affecting the destruction of O_t.

IV. COMPARISON OF MODEL TO DATA

The model above is strongly suggested by the available laboratory data on the radiolysis and photolysis of ice. Here we obtain estimates of σ_d' and σ such as those given in Table I for a few such experiments. We first consider the data for photolysis by ~10 eV photons. We then consider the parameters from the fit to the low-energy electron data and obtain parameters for the energetic ion data.

A. UV photolysis

The results of Gerakines *et al.*[25] confirm that H_2O_2 forms in ice from two OH after a buildup of trapped OH. They monitored the band associated with H_2O–HO,[33] in which the HO is bound to water with ~0.24 eV. Since they monitored a subset of the trapped OH seen in earlier experiments, additional experiments are required. Gerakines *et al.*[25] also found that peroxide production by 9.8 eV photons saturated around 10^{18} photons/cm^2. In addition, HO_2 begins to increase with fluence at about a few times 10^{17}/cm^2 shortly after they begin to detect H_2O_2. However, using Lyman-α photons (10.26 eV) Westley[34] found that O_2 formation was roughly independent of fluence down to ~10^{17} photons/cm^2. Therefore, assuming the states accessible at 9.8 eV are similar to those excited by 10.26 eV, H_2O_2 and HO_2 exhibit a nonlinear dependence on fluence at fluences for which O_2 has reached or is approaching steady state. This comparison, in addition to the lack of a fluence offset [Eq. (5)], suggests that H_2O_2 and HO_2 are unlikely the dominant precursors at low fluences. However, experiments on the same apparatus, at the same temperature and with the same photon energy should be carried out.

The lowest fluence studied by Westley *et al.*[34] also gives a lower limit to the precursor destruction cross section, σ. This is seen to be of the order of the Lyman-α absorption cross section in ice (~0.9×10^{-17} cm^2). Using 9.8 eV photons at low T(12 K) Watanabe *et al.*[29] obtained a cross section for production of D_2 (Table I) at low fluences that is ~10–20% of the total absorption cross section with significant uncertainties. This suggests that $\sigma_d' \approx 0.1$–$0.2\sigma_d$ in the model above, consistent with gas-phase estimates of dissociation water molecules to O. Since photodissociation can produce an excited O, the role of the excess energy in an ice matrix needs to be evaluated.

TABLE I. Parameters for sample data. σ_d' is of the order of 10% of σ_d.

Radiation	E (eV)	T (K)	σ 10^{-16} cm^2	σ_d 10^{-16} cm^2	E_a (eV)
e^-[a]	30–100	50–120	0.8–3	~1	0.02–0.03
$h\nu$[b,c]	~10	~10	≥0.1[c]	0.09[b]	0.03[c]
He^+[d]	10^6	40–140	~10		0.03
Ne^+[e]	1.5×10^6	10	62	≤~35	0.02–0.07

[a]Sieger *et al.*, 1998 (Ref. 2); precursor formation $(0.5–2.0) \times 10^{-18}$ cm^2 (30–100 eV) proportional to $(E-E_0)$, $E_0 \sim 10$ eV, $N \sim 10^{15}$ cm^2.
[b]Watanabe *et al.*, 2000 (Ref. 29); saturation of yield of D_2O ~5×10^{-19} cm^2.
[c]Westley *et al.*, 1995 (Ref. 34); E_a based on D_2O yields, σ based on lowest fluence.
[d]Brown *et al.*, 1982 (Ref. 39); based on lowest fluence.
[e]Reimann *et al.*, 1984 (Ref. 21); σ_d based on $(dE/dx)/W = 92 \times 10^{-15}$ eV cm^2/26 eV.

B. Low-energy electrons

For the low-energy electron data, Sieger *et al.*[2,3] reported an O_2 production cross section of ~2×10^{-18} cm^2 for 100 eV incident electron energy. This is of the order of the electron impact ionization cross section for H_2O, consistent with mobile H or mobile protons as the principal destructive agents.

The O_2 yield versus fluence in these experiments was reasonably well fit by the expression in Eqs. (4). Over a narrow range of T, Sieger *et al.*[2] find $Y_\infty(T) \approx Y_\infty' \times \exp(-E_a/kT)$ with an activation energy $E_a \sim 0.02$–0.03 eV consistent with other estimates of an activation energy. Assuming that in the low-energy electron experiments

N is about 3 ML ($\sim 3\times 10^{15}$ H_2O/cm^2), the measured Y_∞ gives $[\sigma_{O_2}\sigma_p/\sigma]\approx(0.5-2.0)\times 10^{-18}$ cm^2 over the electron impact energy range of 30–100 eV. At 110–120 K, this ratio was found to be proportional to $E-E_o$ for $E>E_o$ ~ 10 eV, again assuming fixed N.[2,3] Using the sizes of σ and Y_∞ then one obtains $[\sigma_p\sigma_{O_2}]\sim(0.2-6)\times 10^{-34}$ cm^2. This size is consistent with both σ_p and σ_{O_2} being described by events of the type $H_2O\rightarrow H_2+O(\sigma_d')$. That is, they are consistent with O being formed for $\sim 10\%$ of the radiation-induced dissociation events ($\sigma_d'\sim 0.1\sigma_d$).

The cross section for production of O may depend on the availability of dangling bonds at interfaces, in pores, or at defects, as suggested by a number of authors. However, the defect and trap densities are critical, as shown here. The role of defects is consistent with the low activation energy and differences observed in the electron-induced yield for initially crystalline and amorphous ice.[3] At relatively high T, the density of initially formed traps becomes small and the mobility of defects is high, so that the sample surface or grain interfaces are the principal trapping sites. For this reason, it is important to determine if the yield for T greater than ~ 140 K depends on the incident flux ϕ, i.e., the dose rate. Pulsed radiolysis experiments in thick ice, in which the transients are studied rather than the steady-state yields, are required.

C. Incident ions: Escape from depth

Even though the shower of secondary electrons produced in a solid by a fast incident ion can result in multiple excitations locally, the yield versus fluence for O_2 production also varies linearly with fluence at low fluences.[21] For low T, this yield is also independent of dose rate at low-dose rates suggesting O_2 formation via a chemical precursor. The O_2 yield versus fluence in Fig. 1(a) for incident ions at low doses can also be roughly fit by the expressions in Eq. (4). However, the fit is not as good as it is for the low-energy electrons suggesting other effects are important. In addition, Y_∞ vs T was shown to have two "plateaus:" one for very low doses and one at higher doses with activation energies in the range $\sim 0.02-0.07$ eV. These differences indicate that additional precursors can be formed in the ion track and that the ion penetration and escape depth for a newly produced O_2 are important. That is, the quantity N in Eq. (1) is the "depth" from which O_2 formed below the surface can percolate to the surface and escape.[35,36] Ignoring these differences and fitting the data for the incident 1.5 MeV Ne^+ at 10 K, one obtains $\sigma=60\times 10^{-16}$ cm^2. This is comparable to size of the molecular destruction cross section, $\sigma_d\approx 30\times 10^{-16}$ cm^2 by these ions (Table I).

At saturation (steady state) a single new event leading to an O can lead to the production O_2 from the steady-state density of trapped precursors in the model proposed here. Therefore, allowing for changes in sample structure, the yield at saturation should be nearly linear in the excitation cross section. This is the case for the low-energy electrons,[2] and it was initially assumed to be the case for the fast ions.[21,37] However, Baragiola *et al.*[38] showed that for a temperature at which decomposition dominates the sputtering of ice,[39] the steady-state yield (Y_∞) is proportional to the square of the electronic energy deposition per unit path length in the solid. If the production and destruction cross sections in Y_∞ in Eq. (4b) roughly scale with $(dE/dx)_e$, the ratio $[\sigma_p\sigma_{O_2}/\sigma]$ also varies as $(dE/dx)_e$. Therefore, we propose that the quantity N in Y_∞ also varies with $(dE/dx)_e$. That is, the depth N from which O_2 can be mobilized to escape depends on the excitation density $(dE/dx)_e$. This is consistent with the observation that the O_2 yield depends on thickness for samples thinner than the ion penetration depth.[21,35] Based on the proposed model, a description of the percolation depth for escape, N, is required to compare the yields for penetrating radiation with those for nonpenetrating radiation. Since the defects/damage produced by the ions can affect both the density of traps and the percolation of O_2, the low-energy electron and UV photons experiments provide better tests of the chemistry for molecular oxygen production.

V. SUMMARY

The exciting observations of thin oxygen atmospheres and oxidants trapped in the icy surfaces on outer solar system bodies[5,6] have lead to increased interest by chemists in the radiation-induced production of oxygen in ice. Although this is a process that has been studied for a half century, quite remarkably, no quantitative model existed. In this paper we first summarized the principal results of those experiments and then give a solid-state chemical model for the production of O_2 in ice *at low doses*. The model is consistent with the available data for formation of oxygen due to electronic excitations in ice produced by fast ions, low-energy electrons, and UV photons at low temperatures.

In our model, trapped oxygen atoms are the dominant precursor to the formation of molecular oxygen at low radiation doses. The proposed rate equations are integrated to obtain an analytic model for the fluence and temperature dependences of the O_2 yield. In deriving the analytic model from the rate equations, the competition between the formation and destruction processes is accounted for. The role of trapping sites and escape from depth for penetrating radiation are also accounted for. These are both affected by the thermal and radiation histories of the sample. This has allowed us to put low-dose data for incident photons, electrons, and energetic ions on the same basis for the first time.

The proposed model suggests measurements that are needed to describe the chemical state of the irradiated ice and to interpret new laboratory data. For instance, the proposed precursor, trapped O, may be detectable. In addition, much more data are needed on the production of oxygen by UV photons, especially as this process is thought to produce the oxygen atmosphere recently observed over Saturn's rings.[5] Studies of possible dose rate affects above ~ 140 K are needed to test the limit of applicability of the trapped precursor model. Studies of the affect of impurities, such as carbon and sulfur species, are needed as these can compete with defect sites to scavenge O. Scavenging by impurities is known to affect the radiolytic yields. This could have been a problem in the earlier experiments but, quite remarkably, more recent results, using ultrahigh vacuum and the vapor

deposition of purified water samples, give similar results. Scavenging by impurities is also of considerable astrophysical interest and has been suggested to be consistent with the observation of primarily oxygen-rich carbon and sulfur species on the icy satellites.[4,6] It has also been suggested[29] that the direct production of H_2 and the production of the precursor[2,22] will be enhanced at the ice surface or at an internal surface in a porous sample. Therefore, the correlation of the formation temperature and radiation damage with the defect density and the formation of trapped O need to be studied in detail. Finally, it is also important to describe quantitatively the relationship between H_2 loss and the competition between O_2 *and* H_2O_2 formations over a range of temperatures and fluences. Such experiments are in progress and the model above will provide a framework for interpreting new data. More importantly, this model can now be used to apply the presently available laboratory data to understanding the observations of molecular oxygen on icy bodies in the outer solar system, an exciting new aspect in planetary science.

ACKNOWLEDGMENTS

Coauthor Dr. T. I. Quickenden died on July 24, 2005. He has contributed significantly to the field dealing with radiation and photochemistry of ices and he will be missed by the community. One of the authors (R.E.J.) acknowledges support from NASA's Geology and Geophysics program and NSF's Astronomy program. Two of the authors (T.M.O. and G.A.G.) acknowledge support from NASA's Planetary Atmospheres Program No. NAG5-13234.

[1] R. E. Johnson and T. I. Quickenden, J. Geophys. Res., [Planets] **102**, 10985 (1997).
[2] M. T. Sieger, W. C. Simpson, and T. M. Orlando, Nature (London) **394**, 554 (1998).
[3] T. M. Orlando and M. T. Sieger, Surf. Sci. **528**, 1 (2003).
[4] R. E. Johnson, T. I. Quickenden, P. D. Cooper, A. J. McKinley, and C. G. Freeman, Astrobiology **3**, 823 (2003).
[5] D. A. Young, J. J. Berthelier, M. Blanc *et al.*, Science **307**, 1262 (2005).
[6] R. E. Johnson, R. W. Carlson, J. F. Cooper, C. Paranicas, M. H. Moore, and M. C. Wong, in *Jupiter: Satellites, Atmosphere and Magnetosphere*, edited by F. Bagenal (Cambridge University Press, Cambridge, UK, 2004).
[7] J. S. Kargel, J. Z. Kaye, J. W. Head III, G. M. Marion, R. Sassen, J. K. Crowley, O. P. Ballesteros, S. A. Grant, and D. L. Hogenboom, Icarus **148**, 226 (2000); C. F. Chyba and K. P. Hand, Science **292**, 2026 (2001); J. F. Cooper, R. E. Johnson, B. H. Mauk, H. B. Garrett, and N. Gehrels, Icarus **149**, 133 (2001).
[8] P. D. Cooper, R. E. Johnson, and T. I. Quickenden, Icarus **166**, 444 (2003).
[9] W. M. Calvin, R. E. Johnson, and J. R. Spencer, Geophys. Res. Lett. **23**, 673 (1996).
[10] J. R. Spencer and W. M. Calvin, Astron. J. **124**, 3400 (2002).
[11] A. U. Khan and M. Kasha, J. Am. Chem. Soc. **92**, 3293 (1970).
[12] R. E. Johnson and W. A. Jesser, Astrophys. J. **480**, L79 (1997).
[13] K. S. Noll, R. E. Johnson, A. L. Lane, D. L. Domingue, and H. A. Weaver, Science **273**, 341 (1996); K. S. Noll, T. L. Roush, D. P. Cruikshank, R. E. Johnson, and Y. J. Pendleton, Nature (London) **388**, 45 (1997).
[14] R. E. Johnson, *Chemical Dynamics in Extreme Environments*, Adv. Ser. Phys. Chem. Vol. 11 (2001), p. 390.
[15] R. W. Carlson, M. S. Anderson, R. E. Johnson *et al.*, Science **283**, 2062 (1999).
[16] G. Vierke and J. Stauff, Ber. Bunsenges. Phys. Chem. **74**, 358 (1970).
[17] A. J. Matich, M. G. Bakker, D. Lennon, T. I. Quickenden, and C. G. Freeman, J. Phys. Chem. **97**, 10539 (1993).
[18] M. T. Sieger, W. C. Simpson, and T. M. Orlando, Phys. Rev. B **56**, 4925 (1997); J. Herring-Captain, G. A. Grieves, A. Alexandrov, M. T. Sieger, H. Chen, and T. M. Orlando, *ibid.* **72**, 035431 (2005).
[19] W. C. Simpson, T. M. Orlando, L. Parenteau, K. Nagesha, and L. Sanche, J. Chem. Phys. **108**, 5027 (1998).
[20] G. A. Kimmel, T. M. Orlando, C. Vezina, and L. Sanche, J. Chem. Phys. **101**, 3282 (1994); G. A. Kimmel and T. M. Orlando, Phys. Rev. Lett. **75**, 2606 (1995); G. A. Kimmel and T. M. Orlando, Phys. Rev. Lett. **77**, 3983 (1996).
[21] C. T. Reimann, J. W. Boring, R. E. Johnson, J. W. Garrett, K. R. Farmer, W. L. Brown, K. J. Marcantonio, and W. M. Augustyniak, Surf. Sci. **147**, 227 (1984).
[22] G. A. Grieves and T. M. Orlando, Surf. Sci. **593**, 180 (2005).
[23] R. R. Rye, T. E. Madey, J. E. Houston, and P. H. Holloway, J. Chem. Phys. **69**, 1504 (1978).
[24] I. A. Taub and K. Eiben, J. Chem. Phys. **49**, 2499 (1968).
[25] P. A. Gerakines, W. A. Schutte, and P. Ehrenfreund, Astron. Astrophys. **312**, 289 (1996).
[26] M. H. Moore and R. L. Hudson, Icarus **145**, 282 (2000).
[27] L. Khriachtchev, M. Pettersson, S. Jolkkonen, S. Pehkonen, and M. Rasanen, J. Chem. Phys. **112**, 2187 (2000).
[28] P. D. Cooper, H. G. Kjaergaard, V. S. Langford, A. J. McKinley, T. I. Quickenden, and D. P. Schofield, J. Am. Chem. Soc. **125**, 6048 (2003).
[29] N. Watanabe, T. Horii, and A. Kouchi, Astrophys. J. **541**, 772 (2000).
[30] M. T. Sieger and T. M. Orlando, Surf. Sci. **390**, 92 (1997).
[31] N. Watanabe and A. Kouchi, Astrophys. J. **567**, 651 (2002).
[32] B. Rowland, M. Fisher, and J. P. Devlin, J. Chem. Phys. **95**, 1378 (1991).
[33] V. S. Langford, A. J. McKinley, and T. I. Quickenden, J. Am. Chem. Soc. **122**, 12859 (2000).
[34] M. S. Westley, R. A. Baragiola, R. E. Johnson, and G. A. Baratta, Planet. Space Sci. **43**, 1311 (1995).
[35] J. Benit and W. L. Brown, Nucl. Instrum. Methods Phys. Res. B **46**, 448 (1990).
[36] P. Ayotte, R. S. Smith, K. P. Stevenson, Z. Dohnalek, G. A. Kimmel, and B. D. Kay, J. Geophys. Res., [Planets] **106**, 33387 (2001).
[37] W. L. Brown, W. M. Augustyniak, L. J. Lanzerotti, R. E. Johnson, and R. Evatt, Phys. Rev. Lett. **45**, 1632 (1980).
[38] R. A. Baragiola, in *Water in Confining Geometries*, edited by J. P. Devlin and V. Buch (Elsevier, New York, in press).
[39] W. L. Brown, W. M. Augustyniak, E. Simmons, K. J. Marcantonio, L. J. Lanzerotti, R. E. Johnson, J. W. Boring, C. T. Reimann, G. Foti, and V. Pirronello, Nucl. Instrum. Methods Phys. Res. B **198**, 1 (1982).